https://dx.doi.org/10.1016/j.tws.2019.106437

Experimental and numerical investigation of concrete-filled hot-finished and cold-formed steel elliptical tubular stub columns

Yancheng Cai [a], Wai-Meng Quach [b,*], Ben Young [c]

[a] Department of Civil Engineering, The University of Hong Kong, Pokfulam Road, Hong Kong, China

[b] Department of Civil and Environmental Engineering, The University of Macau, Macau, China

[c] Department of Civil and Environmental Engineering, The Hong Kong Polytechnic University, Hong Kong, China

(Formerly, Department of Civil Engineering, The University of Hong Kong, Pokfulam Road, Hong Kong, China)

Abstract

The structural behavior of concrete-filled hot-finished (HF) and cold-formed (CF) steel elliptical tubular stub columns was investigated and is presented in this paper. A series of tests was conducted on HF and CF steel elliptical tubular sections infilled with three different concrete grades, namely C40, C80 and C100. The tested HF and CF steel elliptical hollow sections (EHS) had an aspect ratio of 2 with the same nominal section dimension of 200×100×6.5 mm. The test specimens were subjected to uniform axial compression. The initial local geometric imperfection measurements, ultimate loads and failure modes of the concrete-filled HF and CF EHS stub columns are presented. An extensive numerical study accounting for the confinement effect, as well as the non-linearities of materials, geometry and contacts was also performed. After a successful model validation against test results, a parametric investigation was conducted by considering a wide range of the cross-section dimensions and section slenderness of HF and CF EHS with different grades of the infilled concrete. A total of 111 concrete-filled HF and CF EHS specimens were carefully designed and analyzed by using the validated numerical model. The behavior of concrete-filled HF and CF EHS stub columns was investigated, including the maximum load, end shortening, strength enhancement index and ductility index. Effects of section strength factor and column sectional characteristics on the stub-column behavior were also investigated. Furthermore, the experimental and numerical results were used to assess the suitability of the design equations specified in the current American Specifications (AISC and ACI) and European Code (EC4) for the compressive resistance of the concrete-filled HF and CF EHS stub columns. It was found that the predictions from the current international design specifications were overall conservative for both concrete-filled HF and CF EHS stub columns. Generally, the predictions by EC4 were less conservative but more scattered than those predicted by AISC and ACI specifications for the concrete-filled HF and CF EHS stub columns.

Keywords: Cold-formed; concrete-filled steel tubes; elliptical hollow section; experiments; finite element modelling; hot-finished; stub column.

* Corresponding author. Tel.: 853-8822-4358.

E-mail address: wmquach@um.edu.mo (W.M. Quach).

1. Introduction

The axial load carrying capacity and ductility of concrete-filled steel tubular columns can be significantly improved due to the effect of confinement stresses between the steel tube and infilled concrete. This type of columns is increasingly used in high-rise buildings [1]. The Elliptical hollow section (EHS) is a relatively new type of steel tubular sections available in the civil engineering construction. The EHS has a high torsional stiffness and offers different flexural rigidities about the two principal axes, with an efficient bending resistance about the major axis. Hence, it offers a greater bending capacity as compared with a circular hollow section (CHS) of the same area. Furthermore, a reduced visual intrusion can be achieved by using an EHS as compared with a CHS, when viewed from one common direction of the members [2]. These merits of EHS are attractive to engineers and architects, which make it become one of the promising tubular sections in the construction industry. However, the current international steel design specifications [3-8] do not explicitly cover the design of EHS steel members.

There have been an increasing number of studies on the performance of steel members with EHS in recent years. These studies covered a wide range of topics, including the cross-section capacities of stub columns [9], the behavior of beams under bending and combined bending and shear [10, 11], the behavior of columns under pure compression and combined compression and uniaxial bending (about the major axis and minor axis, respectively) [12, 13], welded connections [14, 15] and gusset plate connections [16, 17]. Furthermore, numerical and experimental investigations on concrete-filled steel EHSs were also conducted [18-23]. It should be noted that these investigations focused on hot-finished (HF) and hot-rolled steel EHSs.

Cold forming is one of commonly used manufacturing technologies for steel members. This technology can offer merits including fast manufacturing process, close repetitive tolerance, and high-quality surface finish. Recently, cold-formed (CF) steel tubular members with EHS become available in the market. However, the investigations on the structural behavior of CF EHS are scarce. Recently, Quach and Young [24] conducted an experimental investigation on both the HF EHS and CF EHS which possessed the same nominal dimensions and same virgin material. Their results [24] show that a CF EHS behaves quite differently from a HF steel EHS in terms of resulting mechanical properties after forming. Stress-strain curves for cold-formed steels and hot-rolled steels were investigated and described in [25, 26]. Cai *et al*. [27] conducted both experimental and numerical investigations on the behavior of HF and CF EHS stub columns. It was demonstrated that the modified Direct Strength Method (DSM) [3] proposed by Chen and Young [28] for HF steel EHS stub columns generally gave conservative but reliable predictions. A more recent investigation on concrete-filled CF EHS stub columns was reported by Chan *et al.* [29], Liu *et al.* [30] and Yi and Young [31]. However, these studies [29-31] mainly focused on the behavior of CF EHS specimens only. It should be noted that, up to date, there has been no research focusing on the comparison of the structural behavior between concrete-filled HF and CF EHS stub columns, which is the focus of the present study.

In this study, the structural behavior of concrete-filled HF and CF EHS stub columns was investigated. A series of tests was conducted on HF and CF EHS infilled with three different concrete grades, namely C40, C80 and C100. The HF and CF EHS in the test program had an aspect ratio of 2.0. These test specimens were subjected to uniform axial compression. The initial local geometric imperfection measurements, ultimate loads and failure modes of the concrete-filled HF and CF EHS stub columns are presented. An extensive numerical study accounting for the confinement effect, as well as the

non-linearities of materials and contacts was also performed by using the finite element (FE) method. After a successful FE model validation against test results, a parametric investigation was conducted by considering a wide range of the cross-section dimensions and section slenderness of the HF and CF EHS with different grades of the infilled concrete. A total of 111 concrete-filled HF and CF specimens were carefully designed and analyzed by the validated numerical model. The behavior of concrete-filled HF and CF EHS stub columns was investigated, including the maximum load, end shortening, strength enhancement index (***SI***) and ductility index (***DI***). Effects of column sectional characteristics [i.e., section constraining factor ($\boldsymbol{\xi}$), section aspect ratio ($\boldsymbol{\alpha}$), and section strength factor ($\boldsymbol{\gamma}$)] on the stub-column behavior were also studied. Furthermore, the experimental and numerical results were used to assess the suitability of the current design equations in Specification for Structural Steel Buildings (AISC) [4], European Code (EC4) [32] and Building Code Requirements for Structural Concrete and Commentary (ACI) [33] for the compressive resistance of the concrete-filled HF and CF EHS stub columns.

2. Experimental investigation

2.1 Material properties of steel and concrete

Two different forming processes (i.e., hot finishing and cold forming) are commonly used to fabricate HF and CF steel EHSs, respectively. CF EHSs are fabricated by rolling a steel sheet through a set of rollers into a CHS. The edges of the steel sheet are milled and then closed by welding. The welded CHS is further rolled into an EHS. Except for the welding process, the entire cold-forming process is conducted at the ambient (room) temperature condition. While the hot-finishing process is similar to that of cold forming, except the finishing stage where each EHS is heated to approximately 750 °C or a higher temperature. In the present study, the CF EHS specimens were fabricated by the cold-forming process, while the HF EHS specimens were fabricated by the hot-finishing process. Both the HF EHS and CF EHS specimens were produced from the same virgin steel material [24, 27].

Coupons were cut from a half of each cross-section for the HF EHS and CF EHS specimens, as shown in Fig. 1. Coupon tests were conducted by Quach and Young [24]. Table 1 summarizes the material properties of the HF and CF EHS specimens, including the initial Young's modulus (E_s), static 0.2% proof stress ($f_{0.2}$), static tensile ultimate strength (f_u), elongation at ultimate strength (ε_u), and elongation at fracture (ε_f) based on a 25-mm gauge length. These values covered the locations at the flattest and curviest (corner) of EHS. In addition, the mean values of material properties over the half of the HF and CF EHS specimens were also presented. Unlike those of CF EHS specimens, a distinct yield stress (f_y) was found for each stress-strain curve of HF EHS specimens. Hence, both the $f_{0.2}$ and f_y are presented in Table 1. Details of these coupon test results are described in [24].

The material properties of the concrete were determined by cylinder (150 mm diameter × 300 mm height) tests. The cylinder tests were conducted in accordance with the procedures in the ACI [33]. Three concrete grades (i.e., C40, C80 and C100) with nominal compressive cylinder strengths (f_{ck}) of 40, 80 and 100 MPa were designed using commercially available materials. For each batch of concrete, 3 cylinders were casted and cured under the same environmental conditions. Two concrete cylinders were tested at 28 days and the other cylinder test was carried out at the day of the stub column tests (around 8 months after concrete casting). The mean values of the measured compressive concrete cylinder strengths ($f_{ck,28}$) at 28

days, and the measured cylinder strength ($f_{ck,t}$) at the corresponding day of the concrete-filled stub column tests are presented in Table 2.

2.2 Concrete-filled steel elliptical tubular stub column specimens

2.2.1 Specimen dimension

A series of concrete-filled HF and CF EHS stub columns were experimentally investigated. The HF and CF EHS stub columns had the same nominal cross-section dimensions in this study. The nominal cross-section widths along the major axis ($2a$) and minor axis ($2b$) were 200 mm and 100 mm, respectively. Hence, these EHSs had an aspect ratio of 2.0. The nominal plate thickness (t) of the sections was 6.5 mm. The specimens were cut from the same batch of tubes as those reported by Quach and Young [24]. The nominal length (L) of each EHS tube was taken as 330 mm to make sure that each specimen would not fail by overall buckling. The configuration of the EHS stub column is shown in Fig. 2. The mean values of the measured dimensions of the tubular stub column specimens are summarized in Table 3 [34].

The stub column specimens were labeled by distinguishing their nominal section dimensions and nominal concrete cylinder strengths. For example, Specimen 200×100×6.5-40 indicates that a steel elliptical hollow section has the nominal section dimensions of 200×100×6.5 ($2a$×$2b$×t), and the value following the hyphen is referred to as the nominal concrete cylinder strength of 40 MPa. The symbol "#" indicates that it was a repeated test, as shown in Table 3. All the steel elliptical tubes were wire cut at both ends before infilling concrete. Concrete of different grades was then cast into the steel elliptical tubes and vibrator was also used in the casting process. The nominal concrete cylinder strengths adopted were 40, 80 and 100 MPa as mentioned earlier. Fig. 3 illustrates the prepared concrete-filled HF and CF EHS stub column specimens.

2.2.2 Specimen imperfection

Initial local geometric imperfections of two stub column specimens were measured before infilling the concrete, namely, the HF and CF specimens of 200×100×6.5-80. One Mitutoyo transducer with an accuracy of 0.001 mm was used to inspect the concavity/convexity at five locations (*1*, *2*, *3*, *4* and *5*) on the tube surface along the specimens, as shown in Fig. 4. It was measured along the longitudinal direction of the specimen with a 5 mm interval. The measurements were started and finished 10 mm away from the ends of each specimen, such that the possible local imperfections due to cold sawing can be eliminated. The identical procedure of measurement was performed at five locations (*1*, *2*, *3*, *4* or *5*) for both specimens, as shown in Fig. 4. The measurements were corrected with reference to the datum taken as a straight line connecting the start and end measurement points. The concavity and convexity of the specimen profile are indicated by positive and negative values, respectively. The measured results of the HF and CF specimens 200×100×6.5-80 are shown in Fig. 4. The maximum measured initial local geometric imperfections (w_0) of the two specimens are reported in Table 3. The measured values are close to those of HF and CF EHS stub column specimens reported by Cai *et al*. [27].

2.3 Test setup and procedure

A 5000 kN capacity servo-controlled hydraulic testing machine was used to apply axial compressive force to the concrete-filled HF and CF EHS specimens. Four 50-mm range Linear Voltage Differential Transducers (LVDTs) were used to measure the end shortening of the specimens. These four LVDTs were placed between the top and bottom bearing plates at evenly located positions, as shown in Fig. 5. A total of ten strain gauges were attached on each specimen to determine hoops strain and axial strains at the outer surface of the tube; among which three strain gauges were attached horizontally for hoop strains and seven were attached vertically for axial strains, as shown in Fig. 6. The three strain gauges for horizontal measurements were located at the curviest (corner) locations (No. 1 and No. 3) and flattest location (No. 2) at the middle height of the stub column. The other seven strain gauges (No. 4~10) for vertical measurements were mainly located at one half of the cross-section: three (No. 4~6) were located at the flattest and quarter portions at the middle height of the stub column; another three (No. 7~9) were parallel to those of No. 4~6 along the length direction but located at the quarter height of the stub column; and one strain gauge (No. 10) was located at the curviest (corner) location, which was adjacent to strain gauge No. 3 but for the vertical measurement. The arrangement of these strain gauges was carefully designed to reflect the differences of mechanical properties across the sections, in particular for the CF EHS tubes. The numbering of the strain gauges is shown in Fig. 6.

A typical test setup for the concrete-filled CF EHS stub column is shown in Figure 5. To prevent "elephant foot" failure, a pair of steel frames together with curved steel blocks of 25 mm height was used near each end of the column prior to testing, as shown in Fig. 5. It should be noted that, for the stub columns filled with concrete, the top surface of the column might not be at the same level as the end of the steel tube due to shrinkage of the concrete. Hence, plaster materials (see Figure 5) were used to fill the small gap between the steel tube and infilled concrete. An initial load of approximately 4 kN was applied to the specimens. A special ball bearing was used at the top end of the specimen. During pre-loading, any possible gaps between the specimen and bearing plates were eliminated through rotating the special bearing. The bearing was then locked after pre-loading. These procedures eliminated gaps between the specimen and the contacting surfaces of the testing machine. Thus, the load was applied uniformly across the whole composite cross-section. The load was applied simultaneously to the steel tube and infilled concrete. The displacement control test method was adopted with a constant loading rate of 0.5 mm/min. By using this method, the tests were allowed to be continued after experiencing the peak loads. A data logger was used to record the readings of the LVDTs at 1 second intervals during testing.

2.4 Strengths and curves

The compressive behavior of the stub columns was observed during the tests. The ultimate load ($P_{u,t}$) and the corresponding end-shortening (δ_u), as well as the end-shortening ($\delta_{u,0.85}$) at $0.85P_{u,t}$ after each specimen experienced its ultimate load are shown in Table 4. The test results of the steel EHS stub columns (200×100×6.5-0) without infilled concrete are also included, which have been reported by Cai *et al.* [27]. The applied load versus axial end-shortening relationship was obtained for each column specimen, where the applied load was recorded from the actuator and the end-shortening was measured by the average readings of the LVDTs. Fig. 7 shows the applied load versus end-shortening curves of the concrete-filled HF and CF EHS stub column specimens, as distinguished by the steel type and the nominal infilled concrete strength (e.g., CF-40). One repeated test was conducted on HF-100 specimen,

and the ultimate load of the repeated test was very close to the first test result with a difference of 1.7%. This small difference indicated the reliability of the test results.

Figs. 8 and 9 illustrate the complete load-strain curves for the concrete-filled HF and CF EHS stub columns, respectively. In order to look into the differences of the structural behavior between these two types of sections, the corresponding initial parts of the whole load-strain curves were plotted, as shown in Figs. 10 and 11. The strain gauges of No. 1~3 had positive values due to the Poisson's effect of the tubes, while the strain gauges of No. 4-10 had negative values due to the measurements associated with the axial shortening of the stub columns. Overall, strains obtained from the strain gauges of No. 1~3 and No. 4~10 show consistent trends as loads increased, for both the HF and CF specimens. The strain gauges of No. 1 and No. 10, located at the curviest portion of the section, generally show higher load levels (higher stress levels) than most of other strain gauges under the same strain. The strain gauges of No. 4 and No. 7, located at the quarter of the section perimeter from the curviest portion, show the similar load-strain curves, but generally lower load levels (lower stress levels) than most of other strain gauges under the same strain (see Figs. 10 and 11). Their load-strain curves (No. 4 and No. 7) are not consistent with those from strain gauges of No. 6 and No. 9. Similar differences were found between the load-strain curves for strain gauges of No. 1 and No. 3. In addition, it was also found that the variations of the load-strain curves for CF specimens (see Fig. 11) were relatively larger than those for HF specimens (see Fig. 10). This is due to the material properties of CF EHS varied more obviously than those of HF EHS, as reported by Quach and Young [24]. The non-linearity of the load-strain curves for concrete-filled CF EHS specimens was more obvious than that for concrete-filled HF EHS specimens (see Figs. 10 and 11).

2.5 Failure modes

The failure modes of the tested concrete-filled HF and CF EHS stub columns are shown in Figs. 12 and 13, respectively. The failure modes of CF-0 and HF-0 ("0" means specimens without infilled concrete) steel elliptical tubular stub columns having the same nominal dimensions as those in the present study are also presented. All the concrete-filled HF and CF EHS stub columns failed by the crushing of the infilled concrete together with the steel tubes buckled outwards at some locations. The concrete crushed near the flattest regions of the elliptical sections. It should be noted that the use of steel frames together with curved steel blocks at the ends of the columns is able to prevent the "elephant foot" failure of the specimens. The local buckling failure was observed for both the HF and CF specimens. However, it was clearly shown that the inward local buckling behavior, which occurred in specimens CF-0 and HF-0, was not observed for all the concrete-filled HF and CF EHS stub columns, as it was prevented by the infilled concrete in the steel tubes.

3. Numerical Investigation

3.1 General

Finite element model (FEM) was developed to simulate the tests of concrete-filled HF and CF EHS stub column specimens. The commercial software ABAQUS of version 6.14 [35] was used. A FEM for HF and CF EHS stub columns without infill concrete has been successfully developed by Cai *et al.* [27]. In Cai *et al.* [27], sensitivity analyses were conducted to investigate the effects of important parameters, including element sizes, magnitude of imperfections and mechanical properties across the sections. It was

shown that the FEM based on the material properties at the flattest locations can generally predict the ultimate strengths and failure modes of both HF and CF EHS stub columns but in an accurate and conservative manner [27].

FEMs for concrete-filled steel elliptical tubular stub columns were successfully developed by Dai and Lam [1, 20] and by Liu *et al.* [30], respectively. The stress-strain curves of the confined concrete model in the FEM proposed by Liu *et al.* [30] were firstly validated against their concrete-filled CF steel test specimens [30] with the aspect ratio of $1.0 \leq a/b \leq 2.5$ and the infilled concrete grade C40. The model for concrete-filled steel tubes was also verified with the test results from the literature [18-19, 21, 23, and 29] by Liu *et al.* [30]. The confined concrete model in the FEM proposed by Dai and Lam [20] was firstly validated against the HF steel tubular sections having the aspect ratio of $a/b = 2.0$ with infilled concrete grades C30, C60 and C100 [20]. The confined concrete model was further developed by Dai and Lam [1], and verified with the test results of stainless steel elliptical tubular stub columns with infilled concrete grades C30, C60 and C100 [1]. With consideration of the similar infilled concrete grades and the similar non-linear behavior of the stress-strain curves between CF steel and stainless steel, the stress-strain curves of the confined concrete model proposed by Dai and Lam [1] were adopted in the present study, and were detailed in the following section.

3.2 Confined concrete model

The stress-strain curves of the confined concrete in concrete-filled HF steel and stainless steel elliptical tubular stub columns were developed by Dai and Lam [1, 20]. The maximum strength (f_{cc}) and the corresponding strain (ε_{cc}) of the confined concrete are determined by Eqs. (1)-(3), respectively:

$$f_{cc} = f_{ck} - (6.770 - 2.645(a/b))f_1 \tag{1}$$

$$\varepsilon_{cc} = \varepsilon_{ck}(1 + 20.5f_1/f_{ck}) \tag{2}$$

$$f_1 = f_y \left[e^{-1.3(\frac{a+b}{t})^{0.34}} \right] \tag{3}$$

where f_{ck} is the unconfined compressive cylinder strength; ε_{ck} is the strain corresponding to f_{ck} for unconfined concrete and may be taken as 0.003; f_y ($f_{0.2}$) is the yield strength (0.2% proof stress) of the steel EHS; and f_1 is the strength related to the yield strength and dimensions of the tubular section, which is given by Eq. (3).

Generally, there are four stages for the stress-strain curve of the confined concrete model. The first stage of the stress-strain curve defines the linear property of the confined concrete and the proportional limit stress can be assumed to be $0.5f_{cc}$. The initial Young's modulus (E_{cc}) of the confined concrete is determined by following the empirical formulation provided in ACI [33], where $E_{cc} = 4700\sqrt{f_{cc}}$. The Poisson ratio of the confined concrete is taken as 0.2. The second stage of the stress-strain curve specifies the nonlinear portion which starts from the proportional limit stress $0.5f_{cc}$ and ends at the maximum confined concrete strength f_{cc}. The third stage of the stress-strain curve begins from the maximum confined concrete strength f_{cc} and terminates at the stress corresponding to the strain of $10\varepsilon_{ck}$. The curve continues in the fourth stage and terminates at the stress (> 30 MPa) corresponding to the strain of $30\varepsilon_{ck}$. This confined concrete model proposed by Dai and Lam [1] is applicable to sections with $15 \leq (a+b)/(t) \leq$

65, and $1.0 \leq a/b \leq 2.0$. In the present study, the stress-strain curves of the concrete confined by the CF EHS (200×100×6.5) were constructed based on the Dai and Lam approach [1] and are illustrated in Fig. 14.

3.3 Finite element model and validation

Measured material properties (see Table 1) and measured cross-section geometries (see Table 3) were used in the FEM. As mentioned earlier, the HF and CF EHS specimens were cut from the same batch of tubes as those investigated by Quach and Young [24]. Engineering stress-strain curves for the flattest portions of these tubes, measured in coupon tests, were converted to true stress-true plastic strain curves. Hence, the non-linearity of the material properties was obtained and incorporated into the FEM. The steel tubes and concrete core were modeled using C3D8R solid elements. The C3D8R element is an 8-node linear brick element with reduced integration and hourglass control.

The mesh sizes of concrete with 5~10 mm and steel with 10~20 mm, suggested by Dai and Lam [1], were used in this study. The mesh density of the concrete core is about two times that of the steel tube. The interactive behavior between the steel tube and concrete was simulated using the interaction algorithm in ABAQUS. The inner surface of the steel tube and the outer surface of the infilled concrete were defined to be a contact pair, of which the former acted as slave surface and the latter acted as master surface. Previous investigations [20] have shown that a friction coefficient from 0.1~0.5 generally cause a little effect on the prediction of the ultimate strength, but a smaller friction factor may induce a convergent problem with large deformation. The friction factor of 0.2 or 0.3 was suggested to achieve a quick convergence and to obtain accurate result [20]. Hence, in the present study, the friction factor of 0.2 in the tangential direction between the concrete and steel was used, while the "hard contact" behavior in the normal direction was assumed with no penetration allowed between the surfaces. Local imperfections of steel tubes for concrete-filled steel elliptical tubular stub columns were usually not incorporated in the FEM [1, 20, 30], as the influence of local imperfections is negligible due to the infilled concrete [30, 36]. This has been proved by the sensitivity study for the effects of imperfections on the structural behavior of concrete-filled stainless steel and carbon steel tubular stub columns, as detailed in Tao *et al*. [37, 38]. Hence, unlike the FEM for HF and CF steel elliptical tubular stub columns [27], the initial imperfections of steel tubes were not considered in the FEM for concrete-filled EHS stub columns in the present study.

A reference node located at the centroid of the cross-section for each column end was defined. The reference node was coupled with the corresponding cross-section at each column end in displacements and rotations. Hence, the boundary conditions of each stub column were associated with the reference nodes at both ends. The reference nodes were restrained against all degrees of freedom, except for the longitudinal displacement (along the length direction of the stub column) at the loading point. A specified axial displacement was assigned to the reference node at the loading point. General Static analysis step was adopted. Hence, the adopted displacement control method in the tests was simulated in the FEM analyses. The nonlinear geometric parameter (NLGEOM) was enabled to deal with the large displacement analysis.

Based on the aforementioned confined concrete model and the modelling parameters, the developed FEM was validated against the test results in this study. Table 4 shows the comparison between the ultimate strengths ($P_{u,t}$) from tests and the ultimate strengths ($P_{u,FE}$) from the numerical analysis. It is shown that the developed FEM can successfully replicate the ultimate capacities of the concrete-filled HF and CF steel EHS stub columns, as evidenced by the mean value and COV of $P_{u,t}/P_{u,FE}$ being 0.99 and 0.063, respectively. Figs. 15(a) and 15(b) show the comparisons of load-end shortening curves and failure

modes between tests and FEA for specimens CF 200×100×6.5-100 and HF 200×100×6.5-80, respectively.

4. Parametric studies

4.1 Design of specimens

The validated FEM was used to perform an extensive parametric study on the behavior of concrete-filled HF and CF EHS stub columns. A total of 111 specimens were carefully designed to cover a wide range of fabrication factors, including the cross-section dimensions and slenderness of these EHSs, as summarized in Table 5. The cross-section aspect ratios (a/b) of these EHSs varied from 1.0 to 2.0, with their larger cross-section dimensions ($2a$) varied from 120 to 570 mm. The grades of the infilled concrete were C40, C70 and C100 (i.e., the nominal cylinder strength of 40, 70 and 100 MPa), respectively. The length of each concrete-filled steel stub column (both HF and CF sections) was taken to be 2.0 times the larger outer dimension of the section, as those adopted by Liu *et al.* [30] and by Dai and Lam [1]. The dimensions of concrete-filled HF and CF EHS stub columns used in this parametric study are detailed in Tables 6-9, where the labeling reveals the section dimension ($2a\times2b\times t$) and infilled concrete strength as described in Section 2.2.1. The HF and CF EHS stub columns without infilled concrete are also included, as distinguished by the last segment "0", where these specimens were investigated and reported by Cai *et al.* [27].

The section dimensions for both HF and CF EHS Class 2-4 sections were selected from the sections designed by Cai *et al.* [27]. The section slenderness limits ($D_e/t\varepsilon^2$) specified in EC3-1.1 [7] for CHS were used, where $\varepsilon = (235/f_y)^{0.5}$. The equivalent diameter ($D_e = 2a^2/b$) proposed by Chan and Gardner [9] applicable for $1.0 \leq a/b \leq 4.0$ was adopted to examine the coverage of the cross-section slenderness classification, as the limits are not well defined for EHS in the current international design specifications [3-8]. In the present study, the section slenderness limit of 50, 70 and 90 for $D_e/t\varepsilon^2$ was adopted for the classification of Class 1, Class 2 and Class 3, respectively, as shown in Tables 6-9. In addition, it should be noted that these section dimensions were carefully designed in order to consider the cold-working effect of CF EHS in a conservative manner. As mentioned earlier, the mechanical properties at the flattest portion of the CF steel tube had been used in the validated FEM. The validated FEM was adopted to perform analyses in the parametric study. The forming parameter R_{max}/t (where $R_{max} = a^2/b$) for the tested CF steel tubes is around 32.0 in the present study, which is an indicator of the cold work at the flattest portion of the specimen. A smaller value of R_{max}/t indicates a larger amount of cold work in a section, and thus results in a higher strength enhancement (i.e., a higher 0.2% proof strength $f_{0.2}$). Hence, the dimensions of all the CF specimens in this parametric study were designed such that their values of R_{max}/t are not larger than 32.0, as explained in Cai *et al.* [27]. In this case, the use of the validated FEM (which is based on the mechanical properties at the flattest portion with $R_{max}/t = 32.0$) in the parametric study would result in conservative predictions for CF steel stub columns. Correspondingly, the same section dimensions were selected for the HF sections. However, it should be noted that, as concluded by Quach and Young [24], mechanical properties are uniform across a HF section and the cold-forming effect on the material strength is negligible in HF sections due to the final heat treatment. Hence, the forming parameter R_{max}/t does not affect the material strength of HF sections. Therefore, the dimensions of HF specimens were designed to cover a wider range of the section slenderness in comparison with the CF specimens, regardless of the R_{max}/t value. The dimensions of those HF specimens with $R_{max}/t > 32$ are

shown in Table 9.

4.2 Definition of parameters

As mentioned earlier, the parametric study of the concrete-filled HF and CF EHS stub columns aims to study its axial compressive behavior, [including the maximum load, end shortening, the strength enhancement index (***SI***), and ductility index (***DI***)], as well as the effects of column sectional characteristics [i.e., section constraining factor ($\boldsymbol{\xi}$), section aspect ratio ($\boldsymbol{\alpha}$), and section strength factor ($\boldsymbol{\gamma}$)]. They were described as shown in the following.

The strength enhancement index (***SI***), as expressed in Eq. (4), is defined by the ratio of the ultimate compressive strength (P_u) of the concrete-filled steel tubular stub column to the sum of the strengths of the individual constituent components (i.e., the concrete core and steel tube). The parameter ***SI*** reflects the contribution of composite action in concrete-filled EHS stub columns. In particular, a ***SI*** value higher than 1.0 indicates that the positive interaction between the steel hollow section and the concrete core was achieved. The positive interaction benefits from the confinement effect of the concrete core from the steel tube, as well as the contribution of the concrete core to the delay or elimination of the local buckling in the steel tubular hollow section.

$$\boldsymbol{SI} = P_u/(f_y A_s + f_{ck} A_c) \tag{4}$$

where A_s and A_c are the cross-section area of the hollow section and the concrete core, respectively.

The ductility index (***DI***), as expressed in Eq. (5), is defined as the ratio of the $\delta_{u,0.85}$ to δ_u; where δ_u is the end-shortening at P_u , and $\delta_{u,0.85}$ is the end-shortening at 85% of the P_u after the specimen experiences the P_u. The higher value of the parameter ***DI*** represents that the better ductility of the specimens.

$$\boldsymbol{DI} = \delta_{u,0.85}/\delta_u \tag{5}$$

The section constraining factor ($\boldsymbol{\xi}$), as expressed in Eq. (6), is defined by the ratio of the yield strength of steel hollow section ($f_y A_s$ or $f_{0.2} A_s$) to the compressive strength of the concrete core section ($f_{ck} A_c$). The $\boldsymbol{\xi}$ is one of the factors that may reflect the confinement of steel tube to the concrete core, with the higher value of $\boldsymbol{\xi}$ indicating stronger confinement effect. It should be noted that the actual confinement effect may be affected by other factors, such as the section strength factor ($\boldsymbol{\gamma}$), section aspect ratio ($\boldsymbol{\alpha}$), etc.

$$\boldsymbol{\xi} = (f_y A_s)/(f_{ck} A_c) \tag{6}$$

The section strength factor ($\boldsymbol{\gamma}$) is similar to the ratio of the diameter to wall thickness for a circular hollow section, as expressed in Eq. (7). A higher value of $\boldsymbol{\gamma}$ suggests a weaker section constraining strength and a less confinement to the concrete core due to either the thinner section wall thickness or larger section diameters. The section aspect ratio ($\boldsymbol{\alpha}$) is defined as the ratio of the larger outer dimension to the smaller outer dimension of the elliptical section, as expressed in Eq. (8). This parameter reflects an important feature of the hollow section geometrical shape. For a circular section, $\boldsymbol{\alpha}$ = 1.0. For an elliptical section, $\boldsymbol{\alpha}$ > 1.0. The section aspect ratio may affect the concrete confinement effect.

$$\boldsymbol{\gamma} = (a + b)/t \tag{7}$$

$$\boldsymbol{\alpha} = a/b \tag{8}$$

4.3 Influence of parameters

The parametric study results are presented in Tables 6-9, including $P_{u,FE}$, δ_u and $\delta_{u,0.85}$ for both concrete-filled HF and CF EHS specimens. The stub column specimens without infilled concrete ($2a \times 2b \times t$-0), which have the same nominal section sizes as those specimens with the infilled concrete, are also included in these tables. The areas of the steel tube (A_s) and concrete core (A_c) for each specimen, calculated based on nominal section dimensions, are also presented. The behavior of the concrete-filled HF and CF EHS stub column specimens was investigated in terms of the parameters (***SI***, ***DI***, $\boldsymbol{\xi}$, $\boldsymbol{\alpha}$ and $\boldsymbol{\gamma}$), as shown in Tables 10-13. Furthermore, the ultimate strengths of the specimens with the infilled concrete were normalized by the ultimate strength of the tubular specimen (without infilled concrete) with the same section dimensions and same steel type (i.e., HF and CF) of the tube, as indicated by "*Nor.*" in the Tables 10-13.

Figs. 16 and 17 present the relationships between the strength enhancement index (***SI***) and the infilled concrete strength for different values of the section aspect ratio ($\boldsymbol{\alpha}$) and different cross-section classes of steel tubes, respectively. As shown in Fig. 16, under a given value of $\boldsymbol{\alpha}$ for both concrete-filled HF and CF steel specimens, the value of ***SI*** decreased regularly as the infilled concrete strength increased. A similar decrease of the ***SI*** value with the increment of the infilled concrete strength was found under the same cross-section class of steel tubes for both concrete-filled HF and CF EHS specimens. As shown in Fig. 17, under a given infilled concrete strength for both HF and CF steel tubes, a smaller value of the cross-section slenderness (from slender to compact) generally yielded a better strength enhancement due to the larger ***SI*** value. This is further illustrated in Fig. 18. It is shown that, for both HF and CF specimens, the value of ***SI*** decreased regularly with the increment of the cross-section slenderness ($D_e/t\varepsilon^2$) for the tubes with the same infilled concrete strength. Similar to the relationship between ***SI*** and $D_e/t\varepsilon^2$, the value of ***SI*** decreased as the value of $\boldsymbol{\gamma}$ increased, as shown in Fig. 19. There were some HF specimens with their values of ***SI*** being smaller than 1.0, as shown in Figs. 16-19. These concrete-filled HF specimens (see Tables 9 and 13) possessed much larger values of $D_e/t\varepsilon^2$ for their steel tubes (see Fig. 18); where the confinement for higher concrete grades (i.e., C70 and C100) was not positive, as shown in Figs. 16-18. It may be concluded that hollow sections with larger values of their cross-section slenderness are not suggested to be filled with the concrete of higher grades, as the strength enhancement resulting from the interaction between the steel tube and concrete core would not be achieved under high concrete grades, due to the earlier outward buckling of the outer tube.

The relationship between ***SI*** and $\boldsymbol{\xi}$ is presented in Fig. 20. It was found that, for both the concrete-filled HF and CF EHS specimens, as the value of $\boldsymbol{\xi}$ increased, a better strength enhancement was generally achieved due to a larger value of ***SI***. However, the rate of increment for ***SI*** reduced as the value of $\boldsymbol{\xi}$ increased, and the value of ***SI*** tended to decrease when the value of $\boldsymbol{\xi}$ exceeded 3. As mentioned previously, the ultimate strengths of the specimens with the infilled concrete were normalized by the ultimate strength of the corresponding tubular specimen (without infilled concrete) with the same section dimensions and same steel type (i.e., HF and CF) of the tube, as shown in the Tables 10-13. These normalized column strengths were plotted against the infilled concrete strength associated with different

section aspect ratios of $\boldsymbol{\alpha}$, as shown in Fig. 21; where an infilled concrete strength of "0" in the horizontal axis means the HF or CF EHS specimens without any infilled concrete. By comparing the normalized column strengths of concrete-filled CF EHS specimens with those of concrete-filled HF EHS specimens, it was found that the concrete-filled HF EHS specimens had larger strength increments than the concrete-filled CF EHS specimens, as reflected by either test results or numerical results. The specimens with the section aspect ratio $\boldsymbol{\alpha}$ = 1.0 had larger strength increments than those with $\boldsymbol{\alpha}$ = 1.5 and $\boldsymbol{\alpha}$ = 2.0 for both HF and CF EHS. This is because a steel tube with a circular shape ($\boldsymbol{\alpha}$ = 1.0) can provide a better confinement to the concrete core than sections with other values of $\boldsymbol{\alpha}$. In addition, it was generally found that the normalized column strength increased linearly with the increment of the infilled concrete strength for both HF and CF EHS with a given value of $\boldsymbol{\alpha}$ (see Fig. 22). The ductility indexes (***DI***) of the HF and CF EHS stub columns with and without infilled concrete are shown in Tables 10-13. As shown in these tables, the values of ***DI*** for both concrete-filled HF and CF EHS specimens were generally higher than those without the infilled concrete. These results indicate that the ductility of both the HF and CF EHS specimens in this study was enhanced by the infilled concrete, in particular by the concrete of lower grades (i.e., C40).

5. Assessment of existing design rules

5.1 General

Concrete-filled HF and CF EHS are not explicitly covered by current international design codes. Hence, in the present study, existing design rules for concrete-filled circular hollow sections were used to calculate the nominal strengths of concrete-filled HF and CF EHS stub columns. They include: (1) the "Specification for Structural Steel Buildings" (AISC) [4]; (2) the "Eurocode 4: Design of Composite Steel and Concrete Structures - Part 1.1: General Rules and Rules for Buildings" (EC4) [32]; and (3) the "Building Code Requirements for Structural Concrete (ACI318M-14) and Commentary (ACI318RM-14)" (ACI) [33]. The equivalent diameter ($D_e = 2a^2/b$) proposed by Chan and Gardner [9] was adopted to determine the equivalent diameter of these elliptical hollow sections.

5.2 Specification for Structural Steel Buildings (AISC) [4]

The nominal compressive strength (P_{AISC}) of concrete-filled tubular sections under axial loading is specified in Section I2.1b in AISC [4]. For the cross-section strengths of concrete-filled steel tubular stub columns, sections are categorized as compact, non-compact or slender according to the diameter-to-thickness ($\lambda = D_e/t$) ratios of the outer tubes, as specified in Section I1.4 and Table I1.1a of AISC [4]. This has been discussed and assessed by Lai and Varma [39] and by Wang et al. [40] for composite concrete-filled tubular stub columns. Similarly, in the present study, the value of P_{AISC} was determined by Eqs. (9)-(11):

For compact sections ($\lambda \leq \lambda_p$),

$$P_{AISC} = P_p \tag{9a}$$

$$P_p = f_y A_s + 0.95 f_{ck} A_c \quad (9b)$$

$$\lambda_p = 0.15 E_s / f_y \quad (9c)$$

where P_p is the compressive strength of compact sections; λ_p is the slenderness limit for determining whether a section is compact or non-compact; and E_s, f_y, f_{ck}, A_s and A_c have the same definitions as those described previously in this paper. The outer diameter of the circular section was replaced by the equivalent diameter (D_e) of the elliptical section in the calculation for the present study.

For non-compact sections ($\lambda_p < \lambda \leq \lambda_r$),

$$P_{AISC} = P_p - \frac{P_p - P_y}{(\lambda_r - P_y)^2} (\lambda - \lambda_p)^2 \quad (10a)$$

$$P_y = f_y A_s + 0.7 f_{ck} A_c \quad (10b)$$

where P_y is the compressive strength of non-compact sections; λ_r is the slenderness limit for determining whether a section is non-compact or slender.

For slender sections ($\lambda_r < \lambda$),

$$P_{no} = f_{cr} A_s + 0.7 f_{ck} A_c \quad (11a)$$

$$f_{cr} = 0.72 f_y / (\frac{D_e}{t} \frac{f_y}{E_s})^{0.2} \quad (11b)$$

where f_{cr} is the compressive strength of slender sections. In the present study, all the HF and CF specimens are categorized as compact sections based on the above criteria; except those HF specimens shown in Table 9, which have larger values of the cross-section slenderness.

5.3 Eurocode 4: Design of Composite Steel and Concrete Structures (EC4) [32]

EC4 [32] covers the design rules for encased, partially encased and concrete-filled columns both with and without reinforcements. In the present study, no reinforcement was used in the concrete-filled HF and CF EHS stub columns. It should be noted that concrete grades over C60 are beyond the upper limit as stated in EC4 [32], where the strength classes of the normal weight concrete used in composite members range from C20/C25 to C50/C60 only. The compressive resistance of concrete-filled columns given in EC4 [32] accounts for not only the beneficial confining effect of the steel tube on the concrete, but also the corresponding reduction to the strength of the steel tube caused by those circumferential stresses arising from the restriction of the lateral expansion of the concrete [40]. The simplified design method as specified in Section 6.7.3 in EC4 [32] for concrete-filled circular tubes was adopted in the present study. The nominal strength of a concrete-filled steel circular tubular column (P_{EC4}) can be calculated by Eq. (12):

$$P_{EC4} = \eta_{a0} A_s f_y + A_c f_{ck} [1 + \eta_{c0} \frac{t}{D_e} \frac{f_y}{f_{ck}}] \quad (12)$$

where the steel reduction factor η_{a0} and the concrete enhancement factor η_{c0} for a composite section under pure axial load are given by Eqs. 13(a) and 13(b), respectively:

$$\eta_{a0} = 0.25(3 + 2\bar{\lambda}) \leq 1 \quad (13a)$$

$$\eta_{c0} = 4.9 - 18.5\bar{\lambda} + 17\overline{\bar{\lambda}^2} \geq 0 \quad (13b)$$

where $\bar{\lambda}$ is the relative member slenderness, as defined in EC4 [32]. EC4 [32] considers the confinement effect in circular columns when $\bar{\lambda}$ does not exceed 0.5. The values of $\bar{\lambda}$ are smaller than 0.5 for all the test and numerical specimens in the present study. It should be noted that the effective length factor was equal to 0.5 for all stub columns (with fixed ends) examined in the present study.

A limit on the local slenderness of the outer tube ($D_e/t\varepsilon^2 \leq 90$) is specified in Table 6.3 of EC4 [32], beyond which the local buckling needs to be explicitly accounted for. This limit for concrete-filled tubes is the same as the class-3 slenderness limit for unfilled tubes (i.e., the beneficial effect of the infilled concrete on inhibiting the inward local buckling of the outer tube is ignored). Thus, a further investigation was recommended to determine a more appropriate limit for concrete-filled tubes [40]. In the present study, both the test specimens (shown in Table 3) and numerical specimens (shown in Tables 8-9) exceed the above slenderness limit. Hence, in the present calculation for the cross-section strengths of these specimens, an effective area (A_{eff}) formula [Eq. (14)] proposed by Chan and Gardner [9] was used to replace the area of steel (A_s). This approach was also adopted by Wang *et al*. [40] to determine the cross-section strength of concrete-filled double skin CHS tubular stub columns.

$$A_{eff} = A_s \left[\frac{90}{D_e/_t} \frac{235}{f_y} \right]^{0.5} \quad (14)$$

5.4 Building Code Requirements for Structural Concrete and Commentary (ACI) [33]

Design rules for concrete-filled tubular sections subjected to axial loading are presented in Chapter 10 of the ACI [33]. The ACI [33] neither differentiates among section types, nor makes an explicit allowance for concrete confinement effects. The nominal compressive strength is specified in Section 22.4.2.2 of ACI [33], as shown in Eq. (15):

$$P_{ACI} = A_s f_y + 0.85 A_c f_{ck} \quad (15)$$

It should be noted that the use of the full cross-section area (A_s) for a steel tube requires its thickness to satisfy the condition $t \geq D_e[f_y/(8E_s)]^{0.5}$, as specified in Section 10.3.1.6 of ACI [33]. The thickness of the steel tube should be large enough to attain the longitudinal yield stress before buckling outward [33]. The compressive design resistance of a section beyond this limit is not explicitly covered by ACI [33]. To allow comparisons to be made herein, the effective area (A_{eff}) formula in Eq. (14) was also adopted to account for local buckling in the present study.

5.5 Comparisons with nominal strength predictions

Both test results and FE results (those from the parametric study) of the ultimate strength (P_u) were compared with nominal strengths predicted by the aforementioned code provisions; including AISC [4], EC4 [32] and ACI [33], as summarized in Tables 14(a) and 14(b). Comparisons were performed with all safety factors set to unity.

In the calculation of the nominal strengths (unfactored design strengths) for the test specimens, measured values of the material properties and specimen dimensions were used, which enables a direct comparison between test results and compressive strengths predicted from existing design rules. In calculating the compressive strength, the material properties (f_y and $f_{0.2}$) at the flattest location of the steel elliptical stub section and the concrete cylinder strength ($f_{ck,t}$) at the day of the stub column test were used. As mentioned in Section 2.1, the CF EHS specimens were fabricated by the cold-forming process in this study and the stress-strain curves of cold-worked materials for these specimens did not possess sharp yield points. Therefore, the measured 0.2% proof stress ($f_{0.2}$) was used as the yield strength in calculating the compressive strength for the CF specimens. The measured yield strength (f_y) was used for the HF specimens. For the specimens in the parametric study, the measured f_y and $f_{0.2}$ at the flattest portions of steel EHSs and the nominal f_{ck} of the concrete were used. This is because, in the FE model for the parametric study, measured stress-strain curves of the HF EHS and CF EHS were used together with the stress-strain curves obtained from the confined concrete mode and developed based on nominal concrete strengths. In the comparisons, the mean values for the ratios of the test strength-to-predicted strength and the corresponding coefficient of variation (COV) were determined, and these comparisons are shown in Tables 14(a) and 14(b). Table 14(a) presents the comparison for infilled concrete with different cross-section classes of steel tubes, while Table 14(b) shows the comparison for steel tubes infilled with different concrete grades.

Overall, predictions from the current international design specifications were conservative for both concrete-filled HF and CF EHS stub columns, as the mean values for the ratios of the test strength-to-predicted strength (or FEA-to-predicted strength) were larger than 1.0. Predictions by the EC4 [32] were less conservative than those predicted by the AISC [4] and ACI [33] for both HF and CF specimens, as reflected by smaller mean values (e.g., for CF specimens, the mean values of 1.21, 1.12 and 1.28 for P_u/P_{AISC}, P_u/P_{EC4} and P_u/P_{ACI}, respectively; where P_u represents the ultimate strength $P_{u,t}$ or $P_{u,FE}$). However, the predictions by the EC4 [32] were more scattered than those predicted by the AISC [4] and ACI [33] due to the larger values of COV (e.g., for CF specimens, the COV of 0.097 for the EC4 [32] compared with those of 0.061 and 0.054 for the AISC [4] and ACI [33], respectively). The ACI [33] provided more conservative predictions than the EC4 [32] and AISC [4]. This may be due to the fact that the design method in ACI [33] neither differentiates among cross-sections with various compactness, other than slender sections; nor considers concrete confinement effects. These were further reflected by the comparisons for different cross-section classes of steel tubes (Table 14a) and for different infilled concrete grades (Table 14b). Predictions for the CF specimens were more conservative but less scattered than those for the HF specimens for different international design specifications [4, 32, 33] (e.g., the mean value for P_u/P_{EC4} being 1.12 with the corresponding COV of 0.097 for CF specimens as compared with that of 1.07 with the corresponding COV of 0.105 for HF specimens).

Table 14(a) shows the comparison for concrete-filled steel tubes with different cross-section classes of steel tubes. Generally, it was found that predictions by EC4 [32] were less conservative but more scattered than those predicted by AISC [4] and ACI [33] for those concrete-filled specimens with the same cross-section class of their steel tubes. In general, predictions (for both HF and CF specimens) by

AISC [4] and ACI [33] design specifications were less conservative and less scattered for those concrete-filled with slender tubular sections (Class 4) than those concrete-filled with non-slender sections (Class 2 and Class 3) (e.g., for concrete-filled CF steel tubes with Class 2, Class 3 and Class 4, their mean values of P_u/P_{AISC} being 1.32, 1.23 and 1.18, respectively; and the corresponding COV values of 0.068, 0.051 and 0.044, respectively). However, the predictions by EC4 [32] were more conservative for concrete-filled steel tubes with Class 3 than those concrete-filled steel tubes with Class 2 and Class 4 (e.g., for concrete-filled CF steel tubes with Class 2, Class 3 and Class 4, the mean values of P_u/P_{EC4} being 1.07, 1.14 and 1.11, respectively). Figs. 22(a), 23(a) and 24(a) illustrate comparisons of the test and numerical results with those predicted by AISC [4], EC4 [32] and ACI [33], respectively, for the concrete-filled HF and CF EHS with different cross-section classes of steel tubes. Figs. 22(b), 23(b) and 24(b) present these comparisons in a smaller scale of values for a better illustration with test results.

Table 14(b) shows the comparison for steel tubes infilled with different concrete grades. Similar to the above observation, predictions by EC4 [32] were found to be less conservative but more scattered than those predicted by AISC [4] and ACI [33] for steel tubes infilled with the same concrete grade. Interestingly, for both HF and CF specimens infilled with different concrete grades, the higher infilled concrete grades resulted in the less conservative and less scattered predictions by different design specifications [4, 32, 33] (e.g., for the CF specimens with infilled concrete grades C40, C70 and C100, their mean values of P_u/P_{AISC} being 1.28, 1.20 and 1.17, respectively; and the corresponding COV of 0.059, 0.045 and 0.031, respectively). Figs. 22(c), 23(c) and 24(c) illustrate comparisons of the test and numerical results with those predicted by AISC [4], EC4 [32] and ACI [33], respectively, for the concrete-filled HF and CF EHS with different infilled concrete grades. It is clearly shown that the predictions by AISC [4] and ACI [33] are smaller than (i.e., the underestimation with data above the blue line) the test and numerical strengths of the HF and CF specimens, while the predictions by EC4 [32] are distributed in a more accurate manner, as the data are more evenly distributed near (above and below) the blue line.

6. Conclusions

The structural behavior of concrete-filled HF and CF steel elliptical hollow section (EHS) stub columns has been investigated in the present study. A series of tests was conducted on both HF and CF EHS (with the same nominal section dimensions of 200×100×6.5 mm) infilled with three different concrete grades (i.e., C40, C80 and C100). These HF and CF EHS had an aspect ratio of 2. These test specimens were subjected to uniform axial compression. The initial geometric local imperfection measurements, full load-end shortening curves, load-strain curves, ultimate loads and failure modes of these concrete-filled HF and CF EHS stub columns have been presented in this paper.

An extensive numerical study accounting for the confinement effect, as well as the non-linearities of materials, geometry and contacts have also been performed by using a proposed FE model. A total of 111 concrete-filled HF and CF EHS stub columns were carefully designed and analyzed by the validated numerical model. The behavior of concrete-filled HF and CF EHS stub columns has been investigated, including the maximum load, end shortening, strength enhancement index, and ductility index. Effects of column sectional characteristics and section strength factor on the stub column behavior have also been examined. Finally, experimental and numerical results have been used to assess the suitability of the design equations specified in the current international specifications, including AISC [4], EC4 [32] and

ACI [33] for the cross-section strength of concrete-filled HF and CF EHS stub columns. Findings from the present study are summarized below:

- For specimens with the same section aspect ratio or same cross-section class of steel tubes, the strength enhancement decreases regularly as the infilled concrete strength (up to grade C100) increases.
- For specimens with the same infilled concrete strength, the smaller value of the cross-section slenderness (from slender to compact) or the smaller section strength factor of the tube yields a better strength enhancement.
- A higher section constraining factor generally leads to a better strength enhancement of a specimen. The section constraining factor ranging from 0.27 to 3.82 was examined in this study.
- For specimens with the same value of their section aspect ratios, normalized column strengths (normalized by the strengths of columns without infilled concrete) increase linearly with the increment of the infilled concrete strength. Specimens with the section aspect ratio of 1.0 have larger strength increments than those of 1.5 and 2.0.
- It was found that predictions from the current international design specifications [4, 32, 33] are overall conservative. Generally, predictions by EC4 [4] are less conservative but more scattered than those predicted by AISC [32] and ACI [33] specifications. However, specimens with higher infilled concrete grades generally lead to less conservative and less scattered predictions for these design specifications [4, 32, 33].

Acknowledgements

The authors are grateful to Wo Lee Steel Co. Ltd. Hong Kong for supplying the cold-formed and hot-finished elliptical hollow section test specimens. The research work described in this paper was supported by grants from The Science and Technology Development Fund, Macau SAR (File no. 129/2014/A3) and the Research Grants Council of the Hong Kong Special Administrative Region, China (Project No. 17267416).

References

[1] Dai, X.H. & Lam, D. Axial compressive behavior of stub concrete-filled columns with elliptical stainless steel hollow sections, Steel and Composite Structures, An International Journal 2010; 10:517-539.

[2] Packer J.A. Going elliptical, Modern Steel Construction. March, 2008.

[3] AISI-S100. North American Specification for the design of cold-formed steel structural members. AISI S100-16. Washington,D.C., USA: American Iron and Steel Institute, 2016.

[4] ANSI/AISC 360-16. Specification for Structural Steel Buildings. ANSI/AISC 360-16. Chicago, IL, USA: American Institute of Steel Construction, 2016.

[5] AS4100 1998. Steel structures. AS 4100: Homebush, New South Wales, Australia: Standards

Australia, 1998.
[6] AS/NZS4600 2005. Cold-formed steel structure. AS/NZS 4600:. Sydney, Australia: Standards Australia/Standards New Zealand, 2005.
[7] EC3-1.1. Eurocode 3–Design of steel structures–Part 1.1: General rules and rules for buildings. EN 1993-1-1:2005. Brussels, Belgium: European Committee for Standardization.
[8] EC3-1.3. Eurocode 3–Design of Steel Structures–Part 1-3: General Rules Supplementary Rules for Cold-formed Members and Sheeting, EN 1993-1-3:2006. Brussels, Belgium European Committee for Standardization.
[9] Chan T.M. and Gardner. L. Compressive resistance of hot rolled elliptical hollow sections, Engineering Structures 2008; 30(2): 522–532.
[10] Chan T.M. and Gardner. L. Bending strength of hot-rolled elliptical hollow sections, Journal of Constructional Steel Research 2008; 64(9): 971–986.
[11] Gardner, L., Chan T.M. and Wadee M.A.. Shear response of elliptical hollow sections, Proceedings of the Institution of Civil Engineers, Structures and Buildings, 2008; 161(6): 301–309.
[12] Chan T.M. and Gardner. L. Flexural buckling of elliptical hollow section columns ASCE Journal of Structural Engineering 2009; 135(5): 546–557.
[13] Law K.H. and Gardner L. Buckling of elliptical hollow section members under combined compression and uniaxial bending, Journal of Constructional Steel Research 2013, 86:1-16.
[14] Bortolotti, E.. Jaspart, J.P.. Pietrapertosa, C., Nicaud, G., Petitjean P.D. and Grimault J.P. Testing and modelling of welded joints between elliptical hollow sections, Proceedings of the 10th International Symposium on Tubular Structures, Madrid. Taylor & Francis, London, pp. 259–266, 2003.
[15] Pietrapertosa C. and Jaspart J.P. Study of the behavior of welded joints composed of elliptical hollow sections, Proceedings of the 10th International Symposium on Tubular Structures, Madrid. Taylor & Francis, London, pp. 601–608, 2003.
[16] Willibald S., Packer, J.A., Voth A.P. and Zhao X. Through plate joints to elliptical and circular hollow sections, Proceedings of the 11th International Symposium on Tubular Structures, Quebec City. Taylor & Francis, London, pp. 221–228, 2006.
[17] Willibald S., Packer J.A. and Martinez-Saucedo G. Behavior of gusset plate connections to ends of round and elliptical hollow structural section members, Canadian Journal of Civil Engineering 2006; 33(4): 373–383.
[18] Yang H., Lam D. and Gardner L. Testing and analysis of concrete-filled elliptical hollow sections. Engineering Structures 2008; 30(12): 3771–3781.
[19] Zhao X.L. and Packer J.A. Tests and design of concrete filled elliptical hollow section stub columns. Thin-Walled Structures 2009; 47(6/7): 617–628.

[20] Dai X. and Lam D. Numerical modelling of the axial compressive behavior of short concrete-filled elliptical steel columns. Journal of Constructional Steel Research 2010; 66(7), 931-942.
[21] Uenaka K. Experimental study on concrete filled elliptical/oval steel tubular stub columns under compression. Thin-Walled Structures 2014; 78, 131–137.
[22] Ren Q.-X., Han L.-H., Lam D. and Li, W. Tests on elliptical concrete filled steel tubular (CFST) beams and columns. Journal of Constructional Steel Research 2014; 99: 149-160.
[23] Jamaluddin N., Lam D., Dai X.H. and Ye J. An experimental study on elliptical concrete filled columns under axial compression. Journal of Constructional Steel Research 2013; 87: 6–16.
[24] Quach W. M. and Young B. Material properties of cold-formed and hot-finished elliptical hollow sections. Advances in Structural Engineering 2014; 18(7): 1101-1114.
[25] Gardner L. and Yun X. Description of stress-strain curves for cold-formed steels. Construction and Building Materials 2018; 189 (20): 527-538.
[26] Yun X. and Gardner L. Stress-strain curves for hot-rolled steels. Journal of Constructional Steel Research 2017; 133: 36-46.
[27] Cai Y., Quach W.M., Chen M.T. and Young, B. Behavior and design of cold-formed and hot-finished steel elliptical tubular stub columns. Journal of Constructional Steel Research 2019; 156: 252-265.
[28] Chen M.T. and Young B. Material properties and structural behavior of cold-formed steel elliptical hollow section stub columns. Thin-Walled Structures 2019; 134: 111–126.
[29] Chan T.M., Huai Y.M. and Wang W. Experimental investigation on lightweight concrete-filled cold-formed elliptical hollow section stub columns. J. Constr. Steel Res. 2015; 115:434–444.
[30] Liu F., Wang Y., and Chan T.M. Behavior of concrete-filled cold-formed elliptical hollow sections with varying aspect ratios. Thin-Walled Structures 2017; 110: 47-61.
[31] Yi S. and Young, B. Tests of concrete-filled steel stub columns with cold-formed and hot-finished elliptical section. Proceedings of the 16th International Symposium on Tubular Structures (ISTS16), Taylor & Francis, Melbourne, Australia, pp. 109-115, 2017.
[32] EC4. Eurocode 4: Design of Composite Steel and Concrete Structures - Part 1.1: General Rules and Rules for Buildings, EN 1994-1-1:2004. Brussels, Belgium European Committee for Standardization, Belgium, 2004
[33] ACI 318-14, “Building code requirements for structural concrete (ACI 318M-14) and commentary (ACI 318RM-14)”, American Concrete Institute, Detroit, USA, 2014.
[34] Cai Y., Quach W.M. and Young B. Tests of concrete-filled cold-formed and hot-finished steel elliptical tubular stub columns. The 8th International Conference on Thin-Walled Structures, Lisbon, Portugal, 2018, Paper No. 34, Full paper in USB.
[35] ABAQUS analysis user's manual, Version 6.14. ABAQUS, Inc.; 2017.

[36] Tao Z., Wang Z.-B. and Yu Q. Finite element modelling of concrete-filled steel stub columns under axial compression. Journal of Constructional Steel Research 2013; 89: 121–131.
[37] Tao Z., Uy B., Liao F.-Y., and Han L.-H. Nonlinear analysis of concrete-filled square stainless steel stub columns under axial compression. Journal of Constructional Steel Research 2011; 67: 1719–1732.
[38] Tao Z., Uy B., Han L.-H. and Wang Z.-B. Analysis and design of concrete-filled stiffened thin-walled steel tubular columns under axial compression. Thin-Walled Structures 2009; 47: 1544–1556.
[39] Lai Z. and Varma A. H. High-Strength Rectangular CFT Members: Database, Modeling, and Design of Short Columns. Journal of Structural Engineering (ASCE) 2018; 144(5): 04018036.
[40] Wang F., Young B and Gardner L. Compressive testing and numerical modelling of concrete-filled double skin CHS with austenitic stainless steel outer tubes. Thin-Walled Structures 2019; 141:345-359.

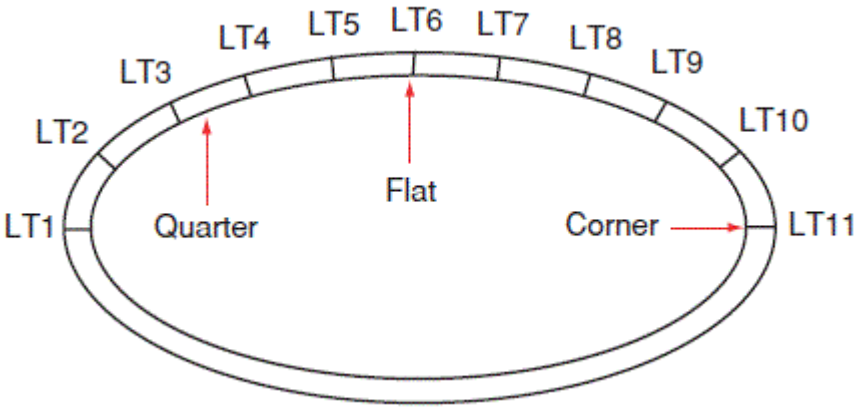

Figure 1: Location of coupon specimens tested across the section [24]

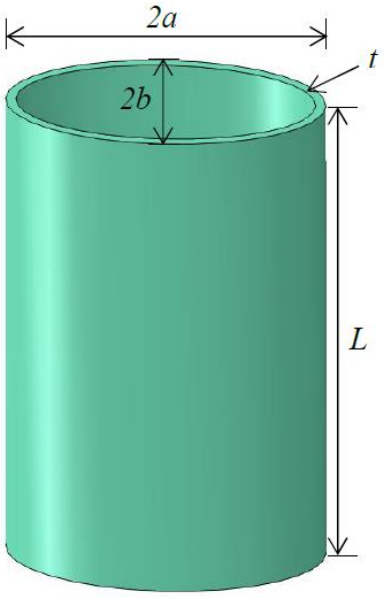

Figure 2: Configuration of an elliptical tubular stub column

Figure 3: Prepared concrete-filled stub column specimens with strain gauges

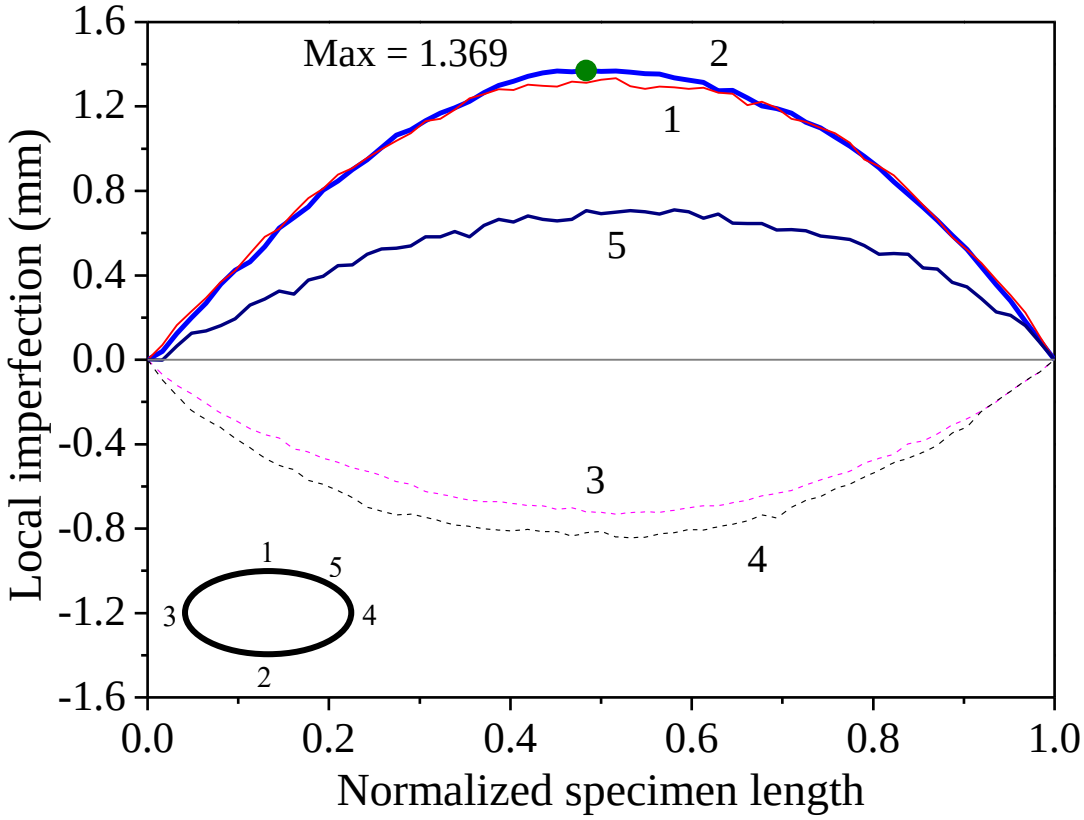

(a) Specimen of CF steel tube [34]

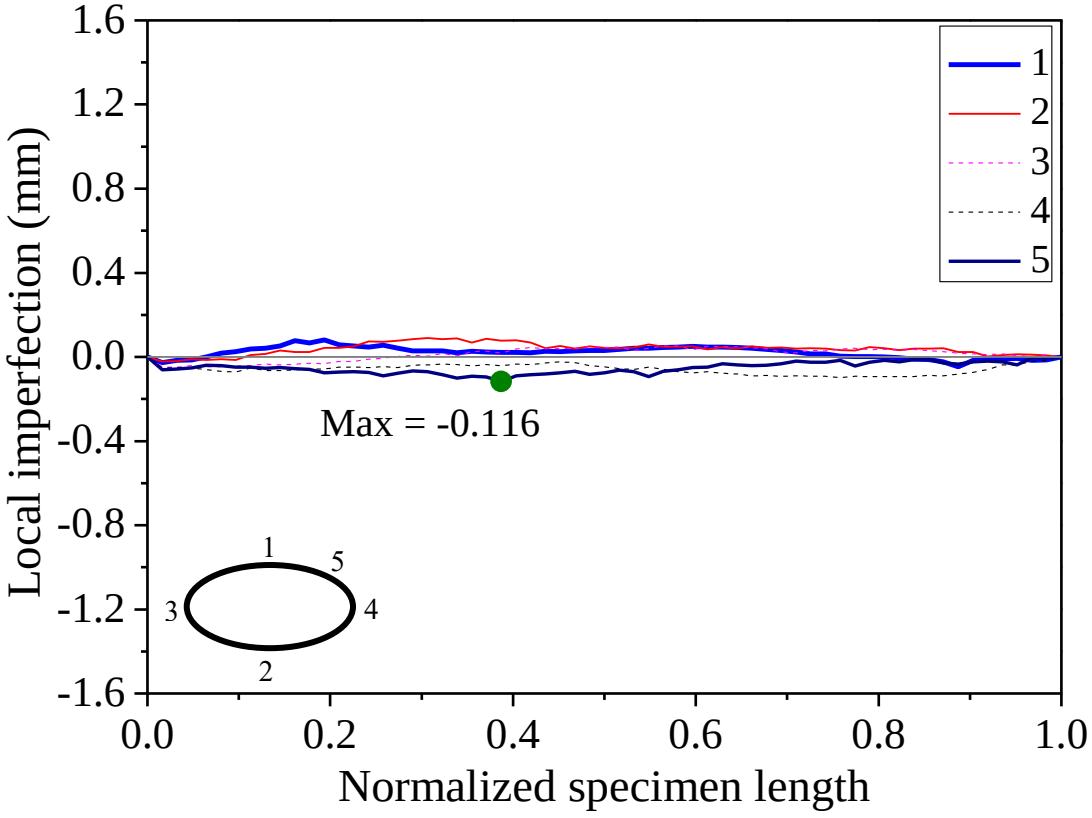

(b) Specimen of HF steel tube

Figure 4: Measured local imperfection profile for specimen Series 200×100×6.5-80

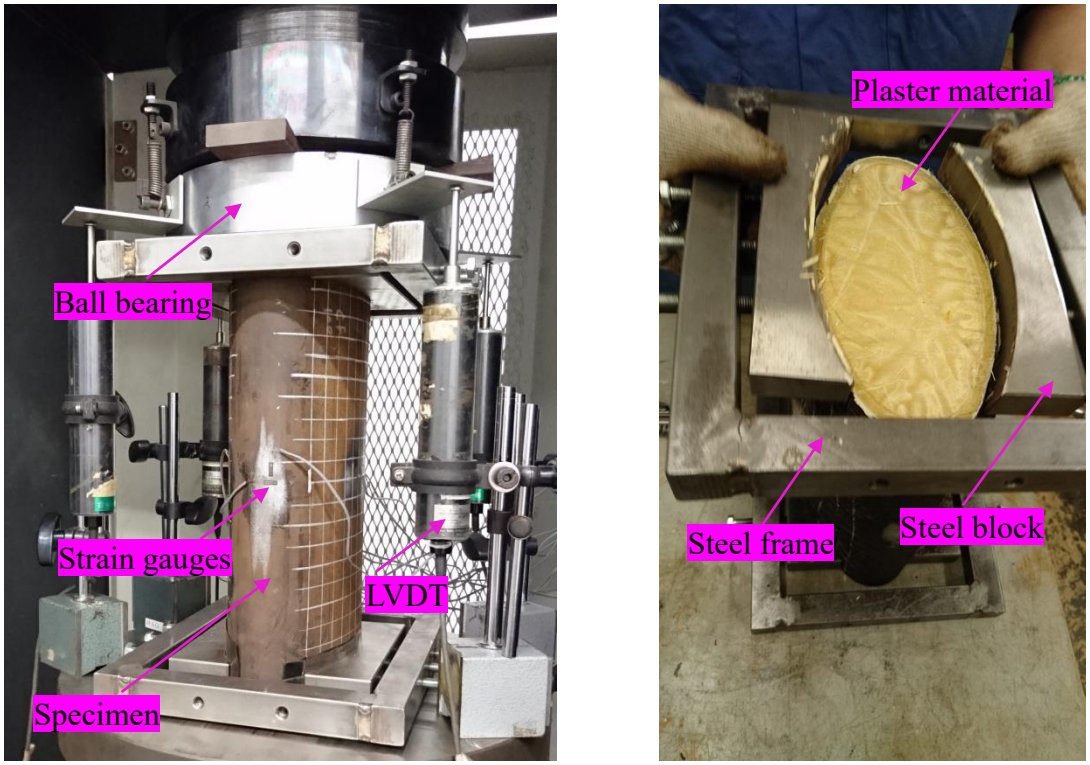

Figure 5: Specimen CF 200×100×6.5-100 during testing (left) and after testing (right)

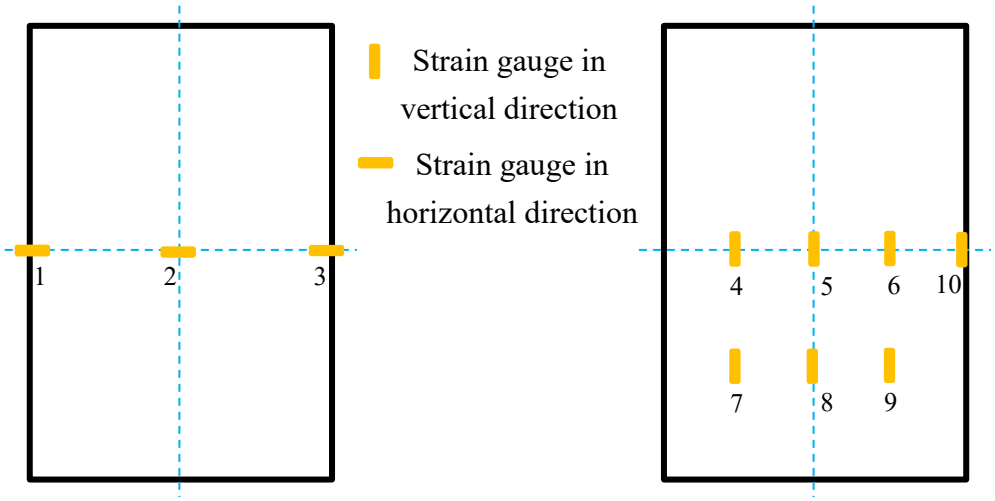

Figure 6: Arrangement and numbering of strain gauges in the stub column specimens (elevation view)

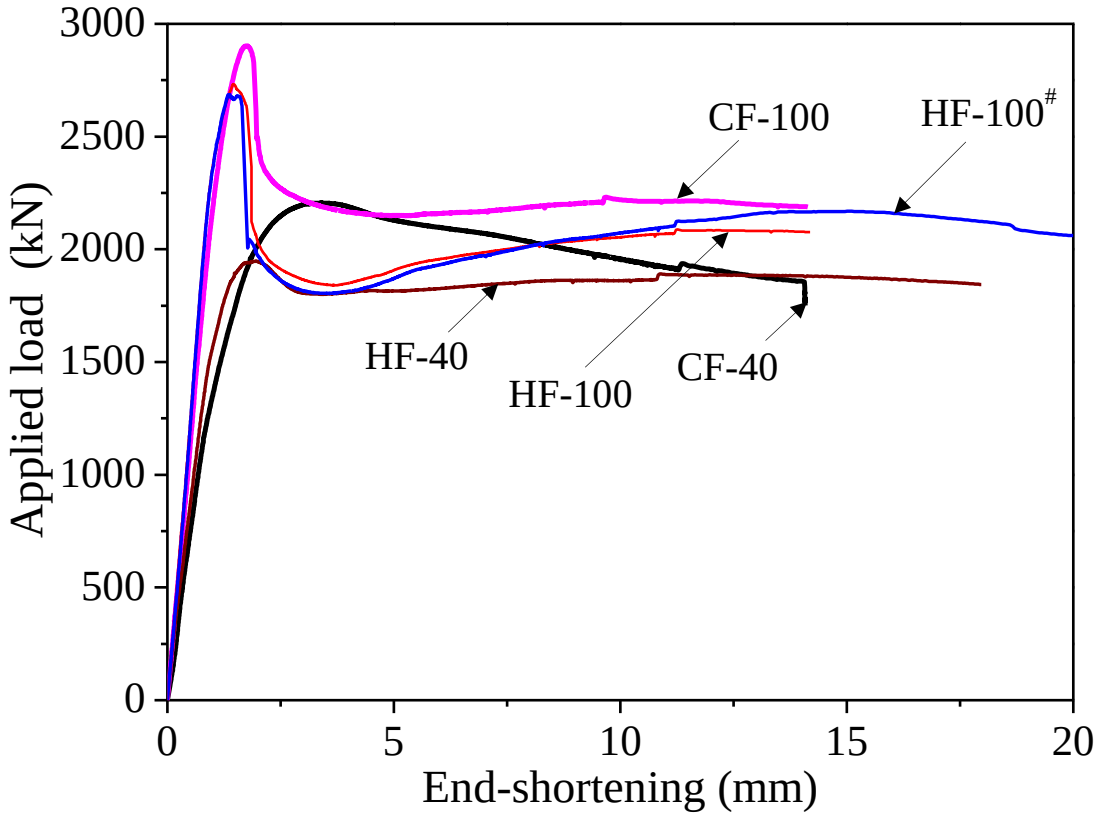

Figure 7: Load versus end-shortening curves for different specimen series by tests

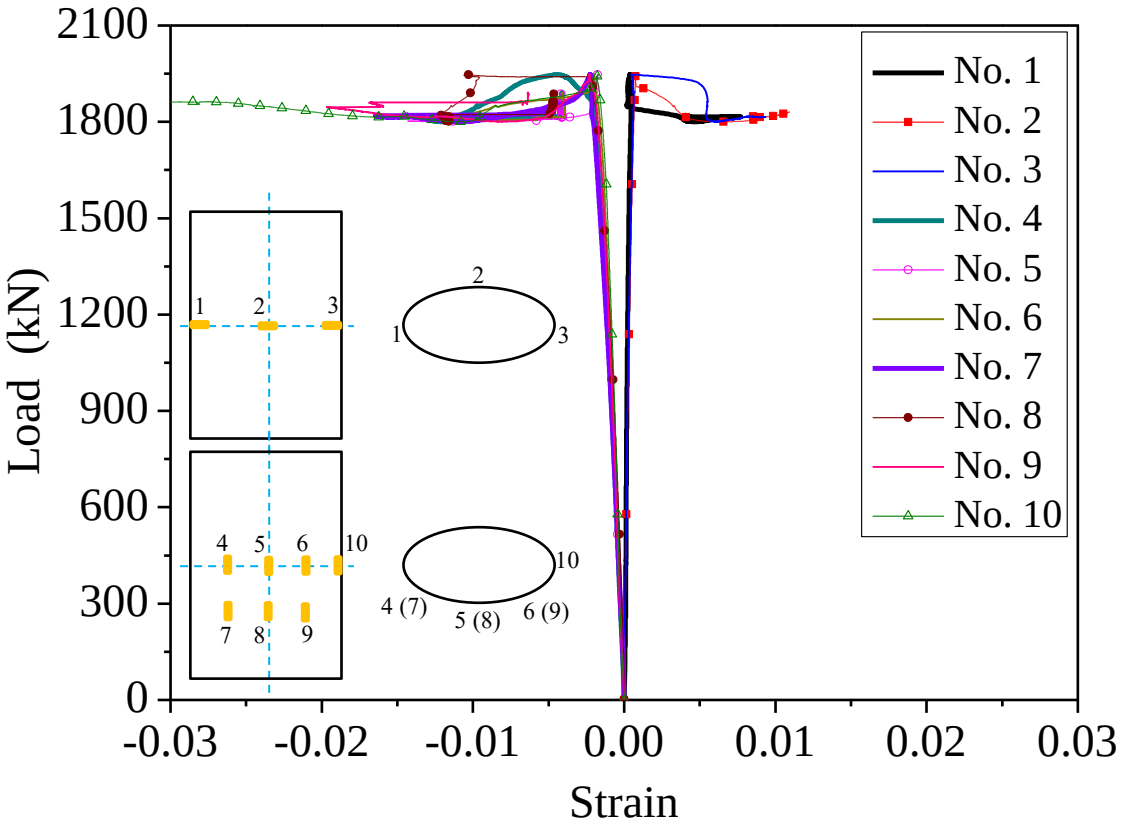

(a) Specimen HF-40

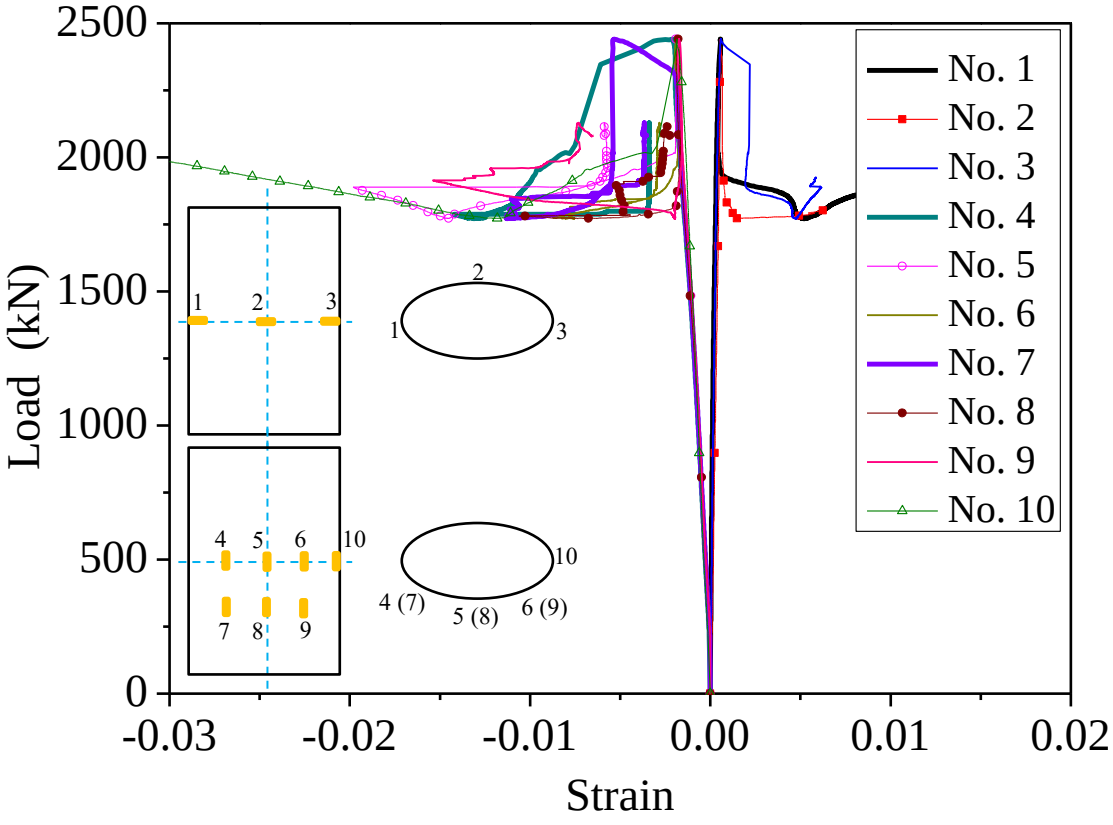

(b) Specimen HF-70

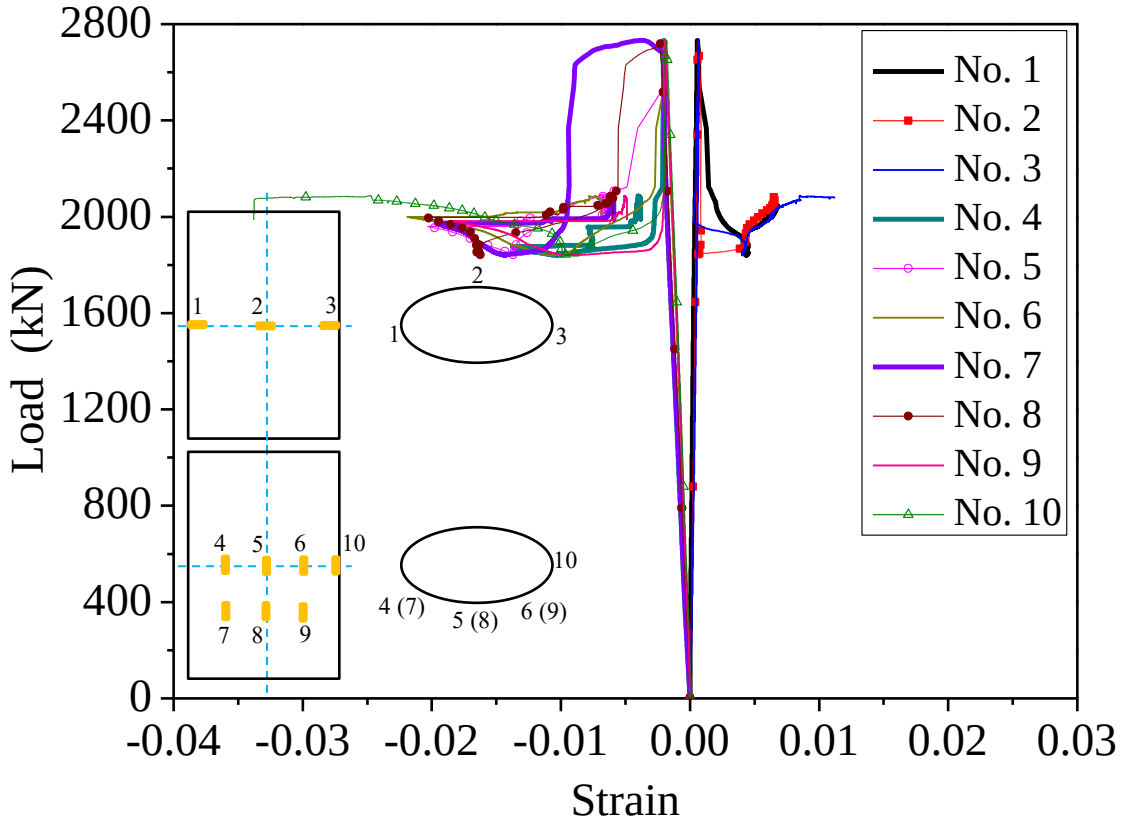

(c) Specimen HF-100

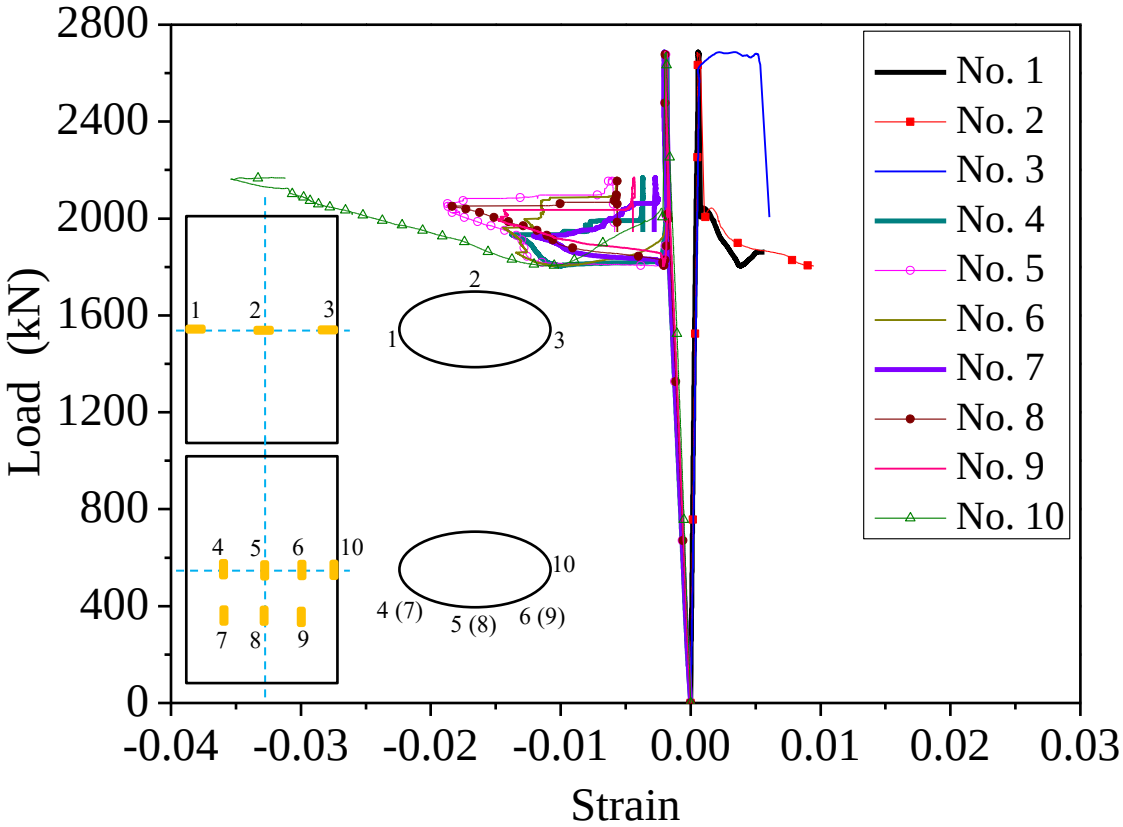

(d) Specimen HF-100#

Figure 8: Complete load-strain curves for hot-finished (HF) specimens

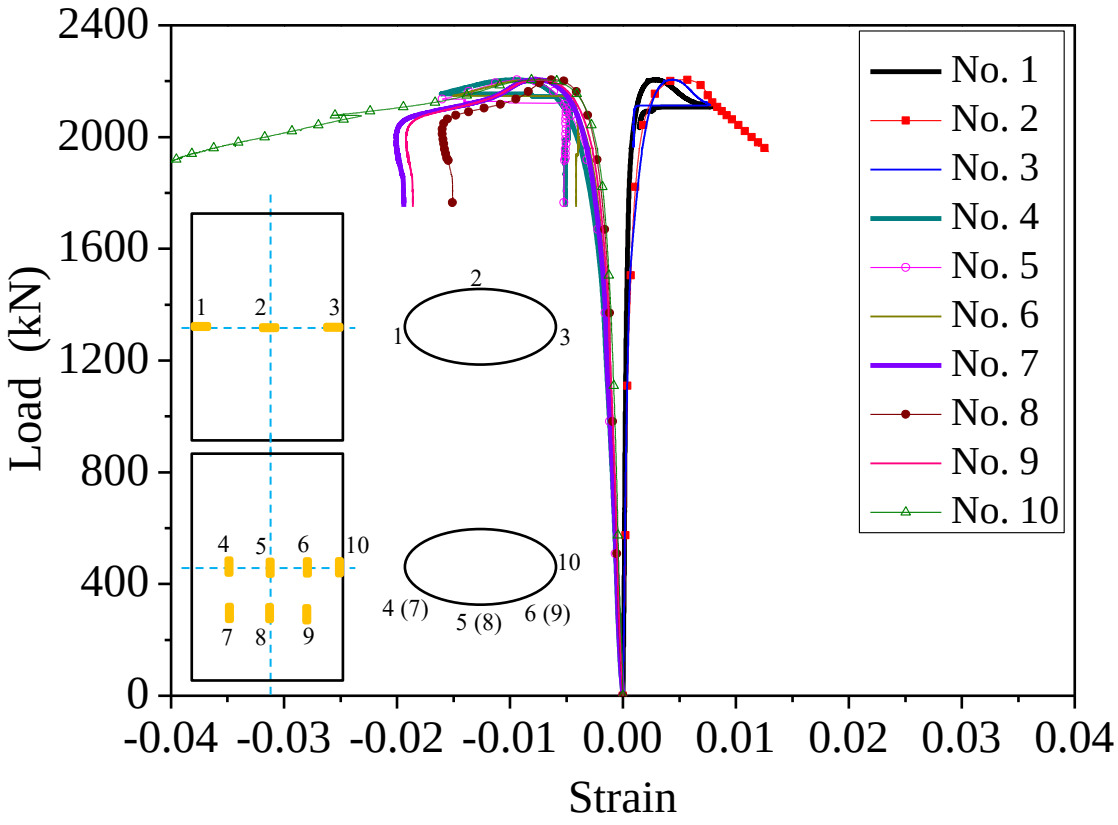

(a) Specimen CF-40

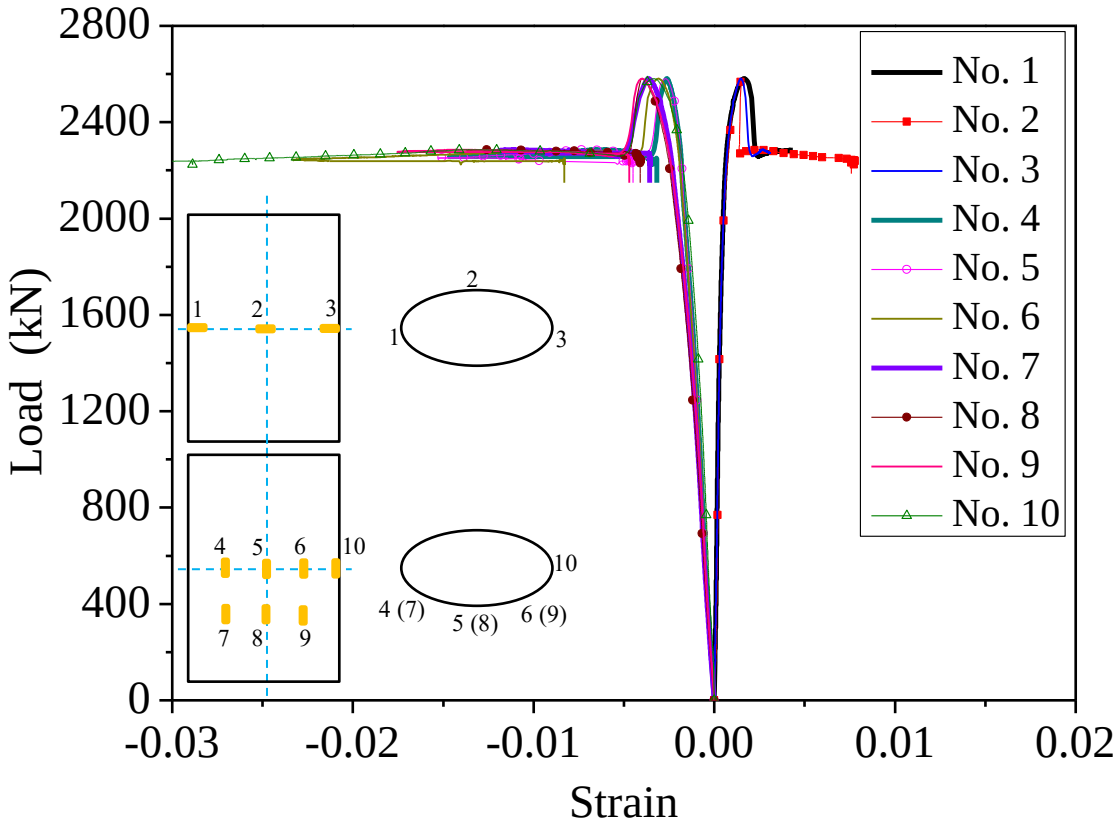

(b) Specimen CF-70

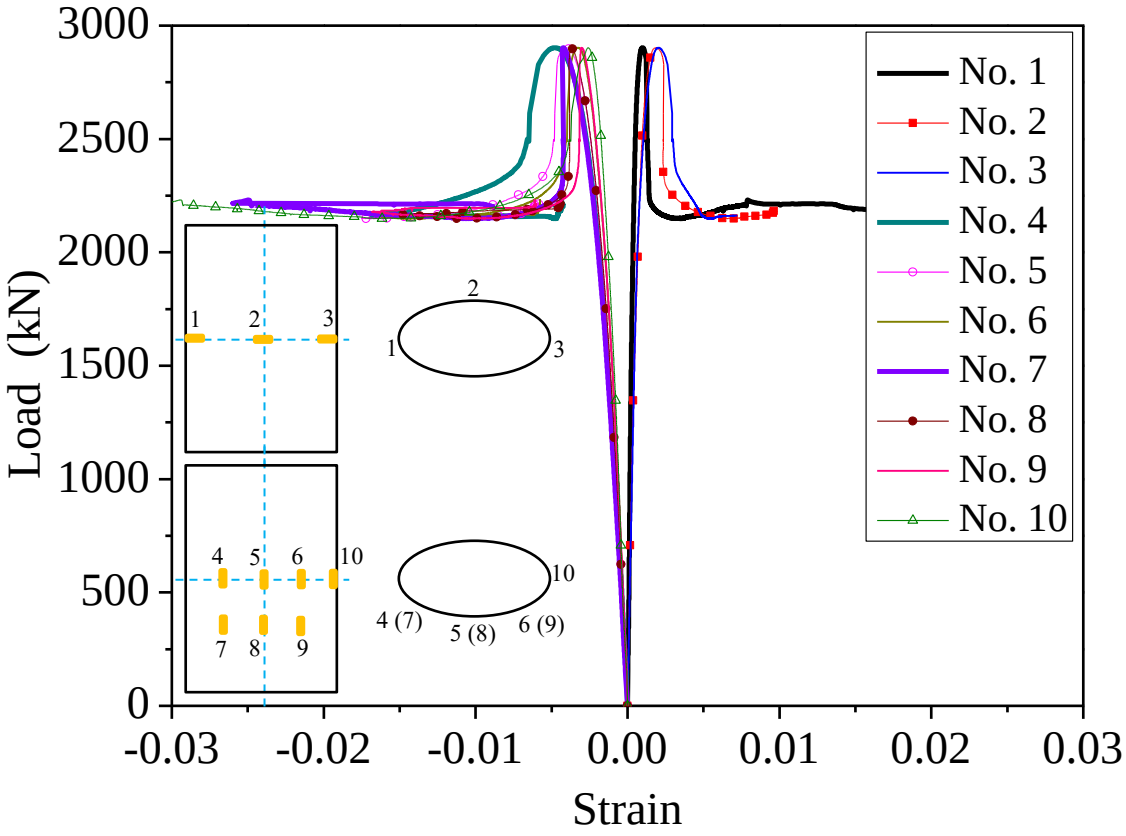

(c) Specimen CF-100

Figure 9: Complete load-strain curves for cold-formed (CF) specimens

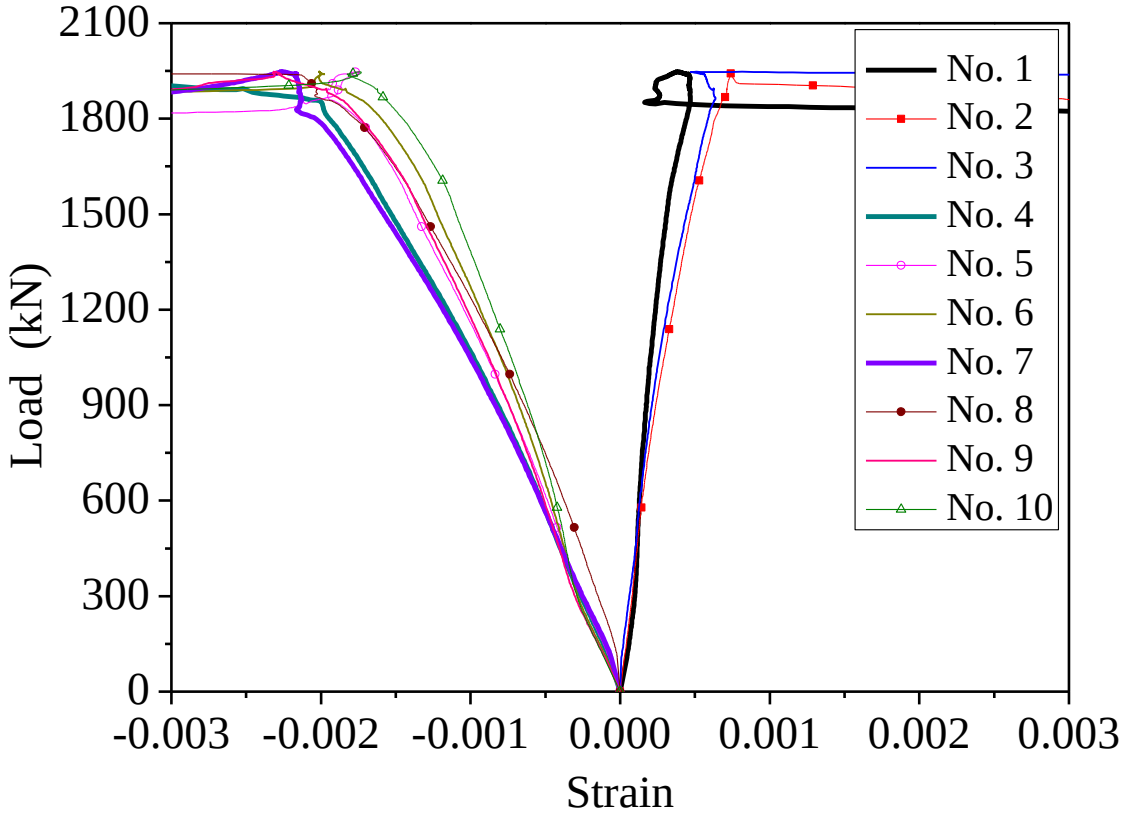

(a) Specimen HF-40

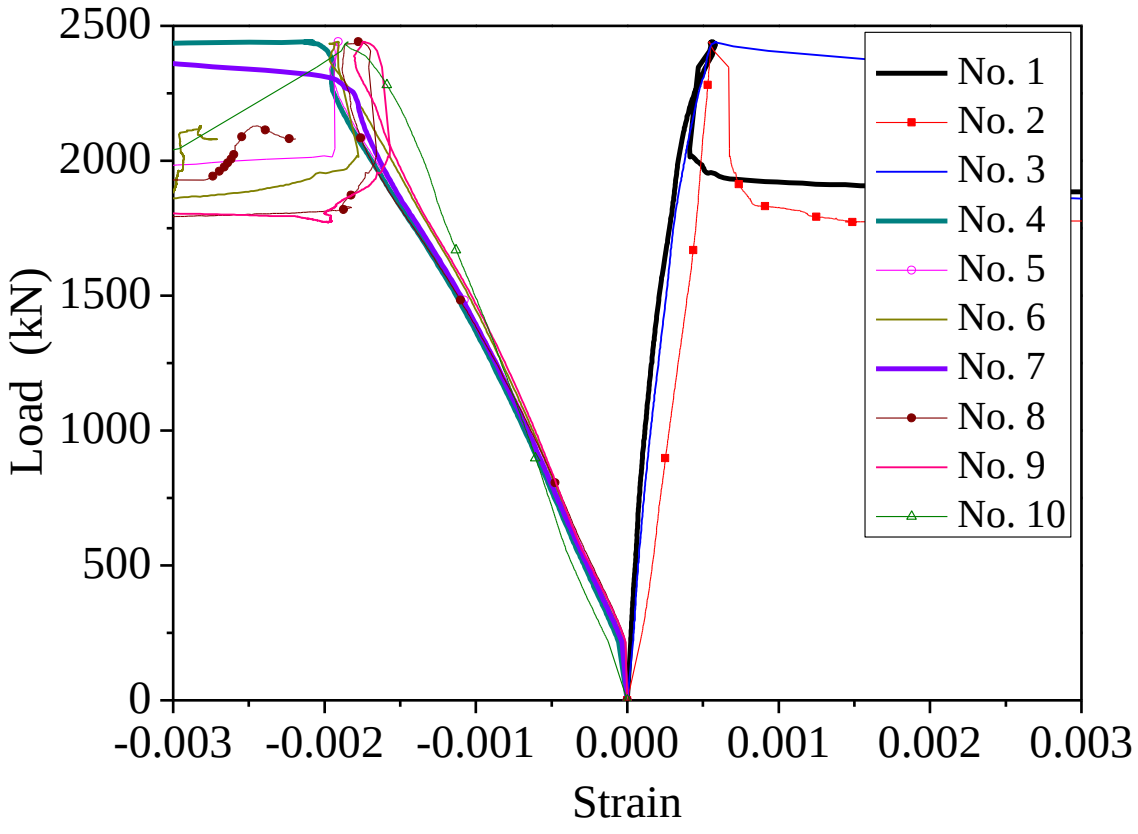

(b) Specimen HF-70

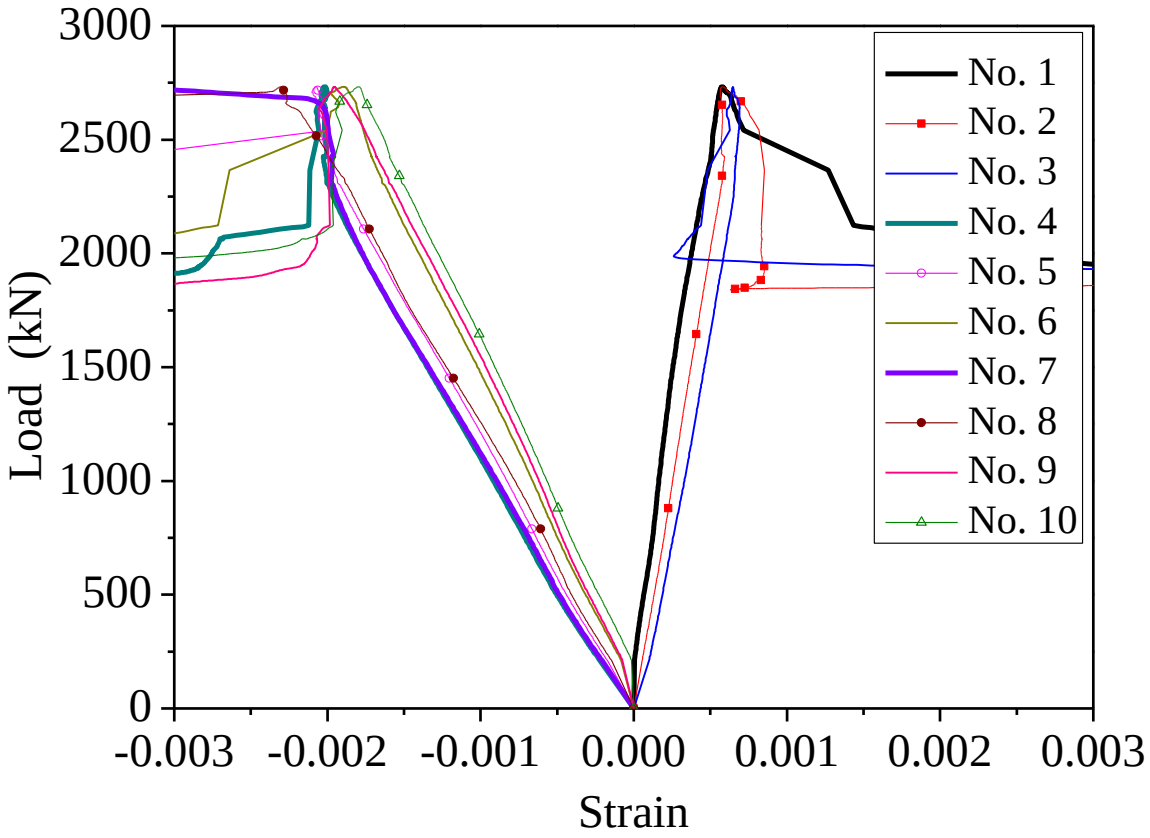

(c) Specimen HF-100

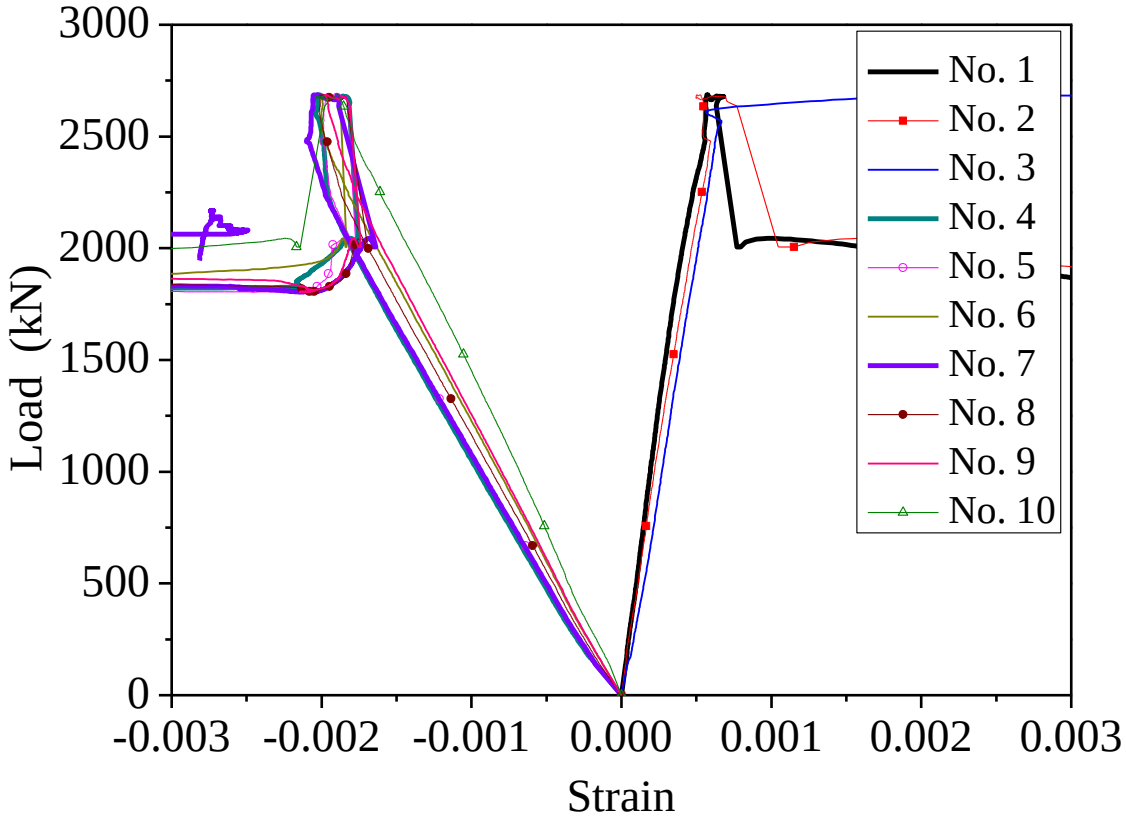

(d) Specimen HF-100#

Figure 10: Initial load-strain curves for hot-finished (HF) specimens

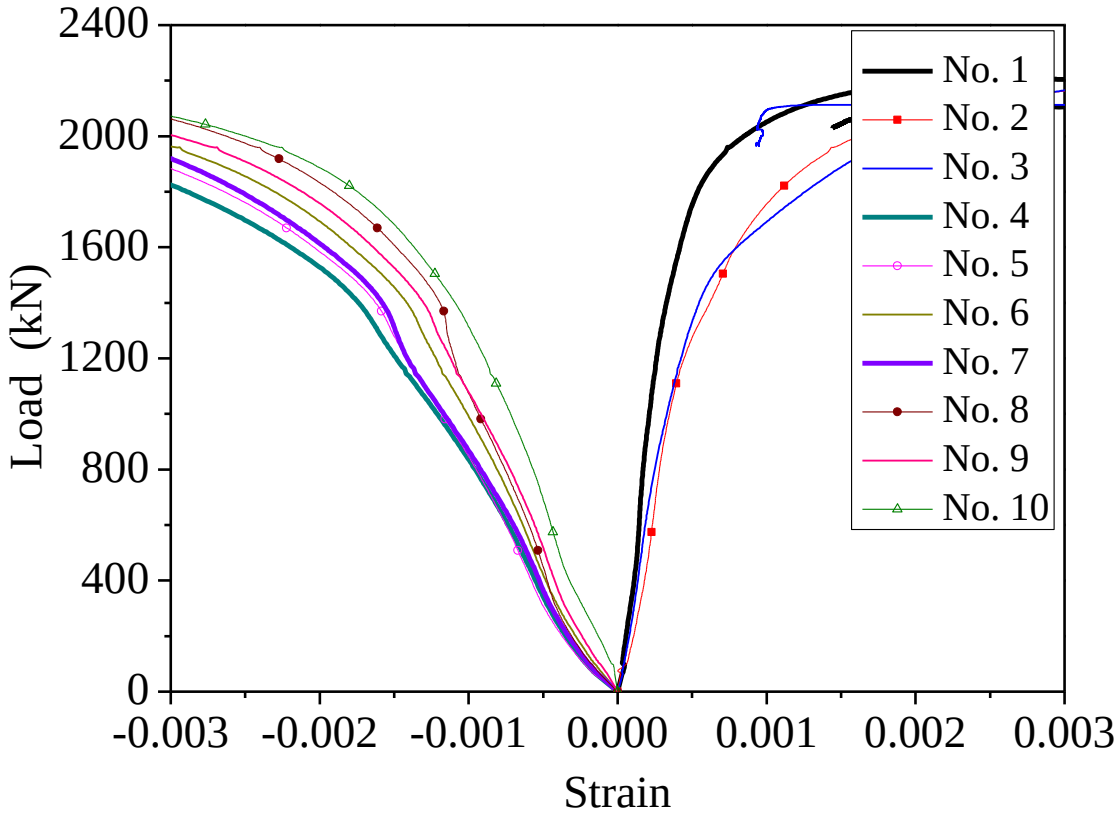

(a) Specimen CF-40

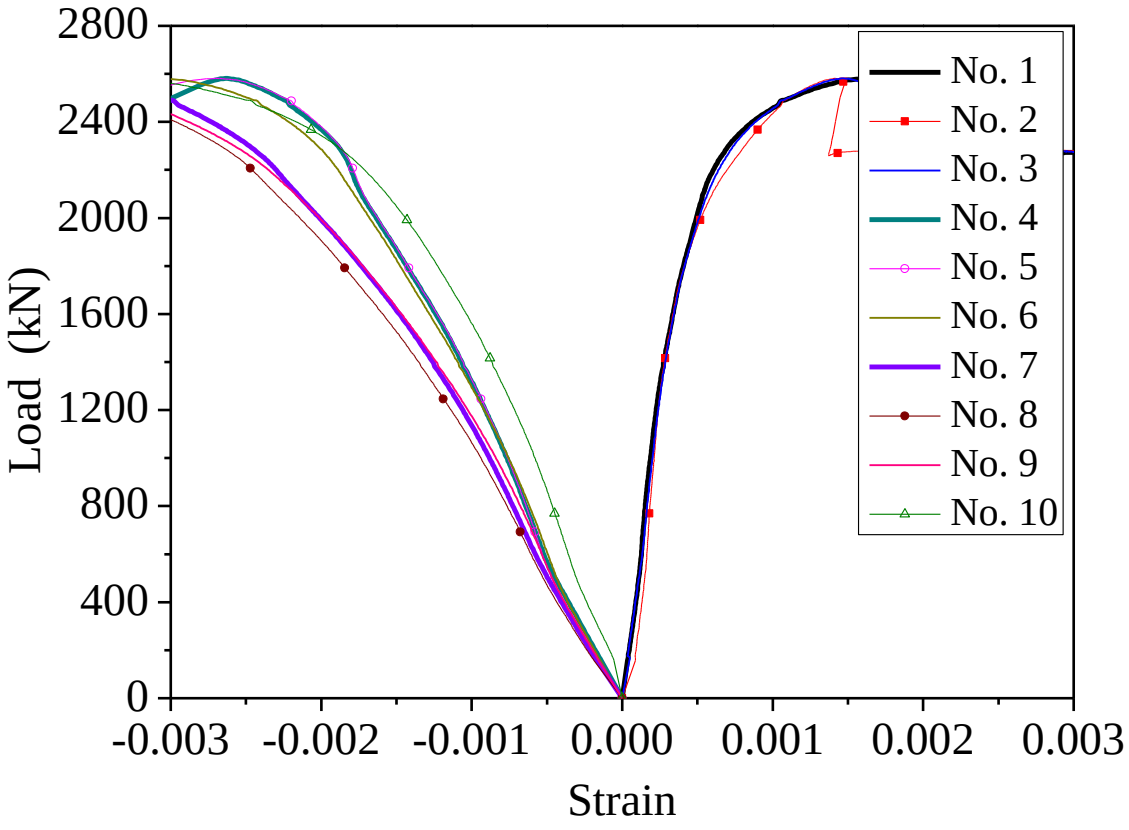

(b) Specimen CF-70

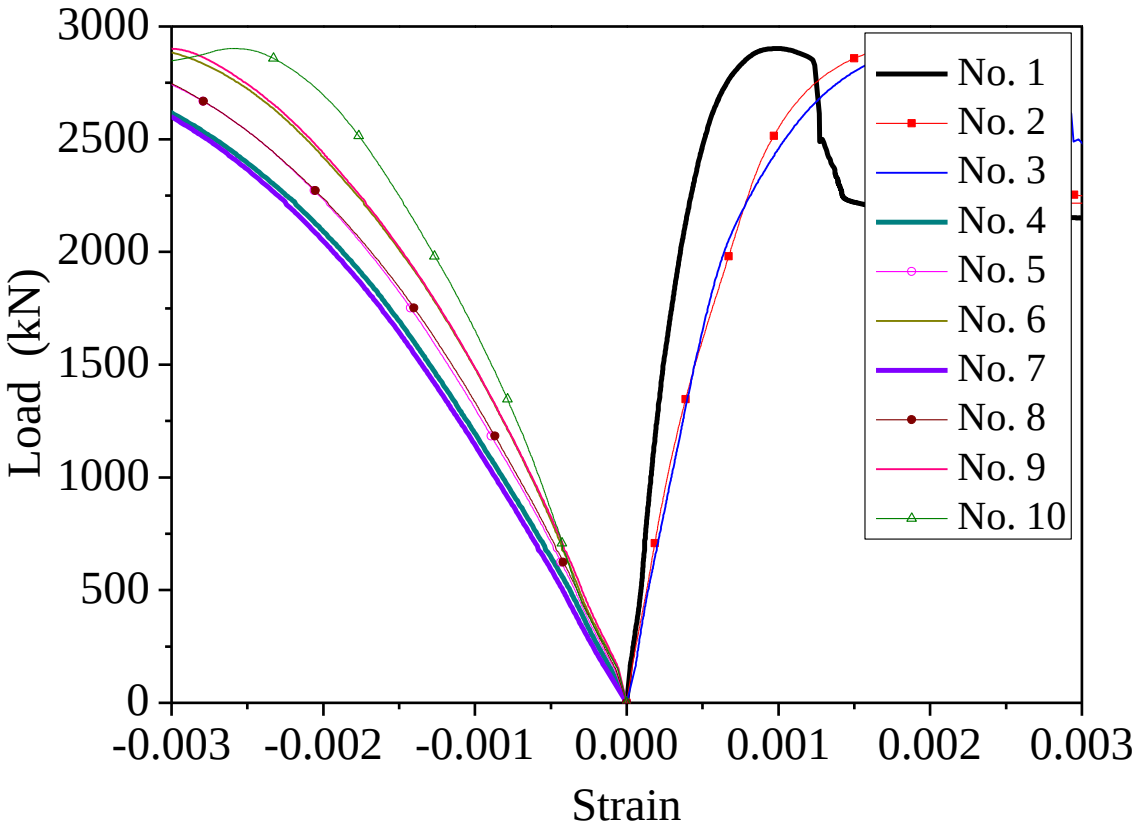

(c) Specimen CF-100

Figure 11: Initial load-strain curves for cold-formed (CF) specimens

a) HF-0 b) HF-40 c) HF-80 d) HF-100

Figure 12: Failure modes of specimen Series HF 200×100×6.5 [34]

a) CF-0 b) CF-40 c) CF-80 d) CF-100

Figure 13: Failure modes of specimen Series CF 200×100×6.5 [34]

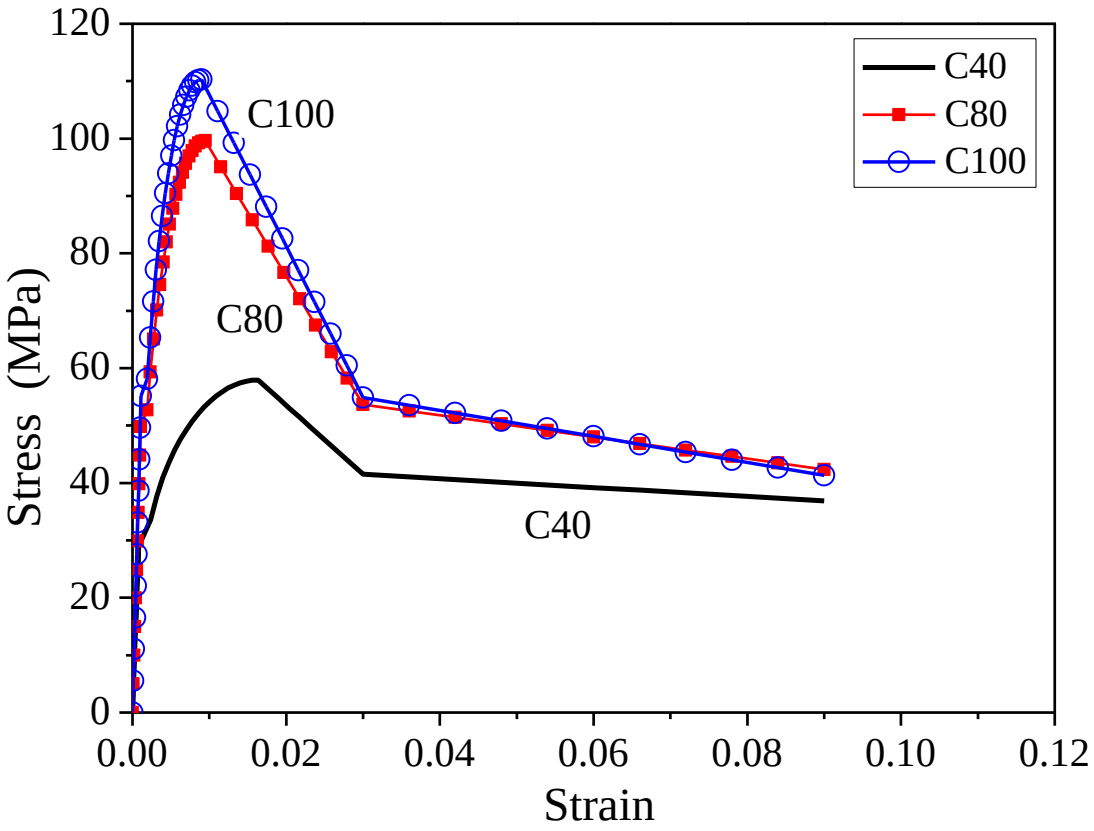

Figure 14: Stress-strain curves of concrete confined by CF EHS in the tests

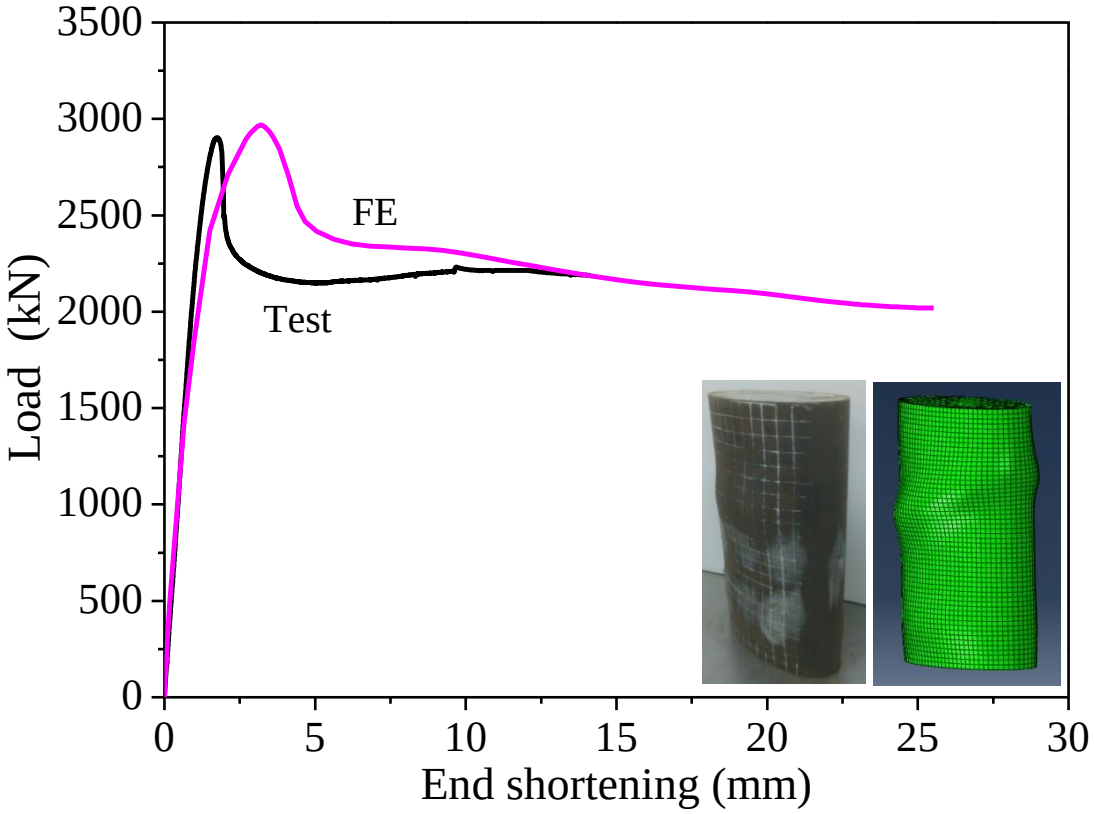

(a) Specimen CF 200×100×6.5-100

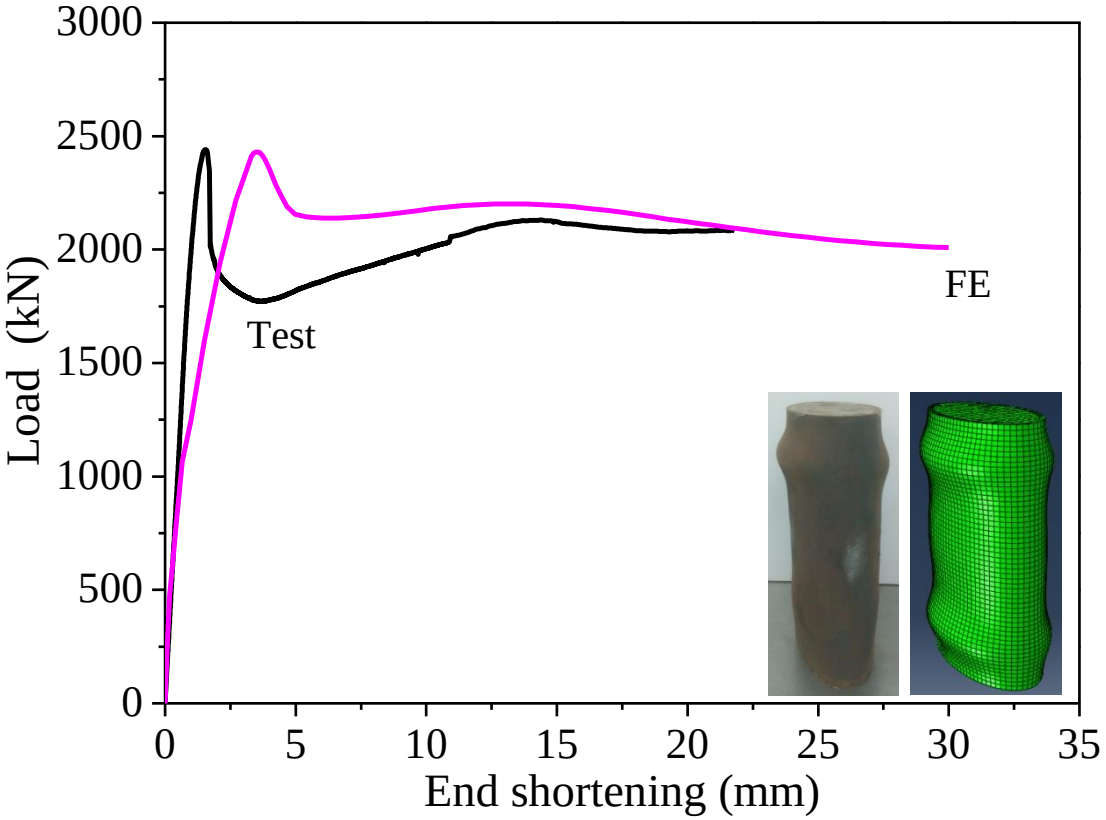

(b) Specimen HF 200×100×6.5-80

Figure 15: Comparison of load-end shortening curve and failure mode between test and FEA

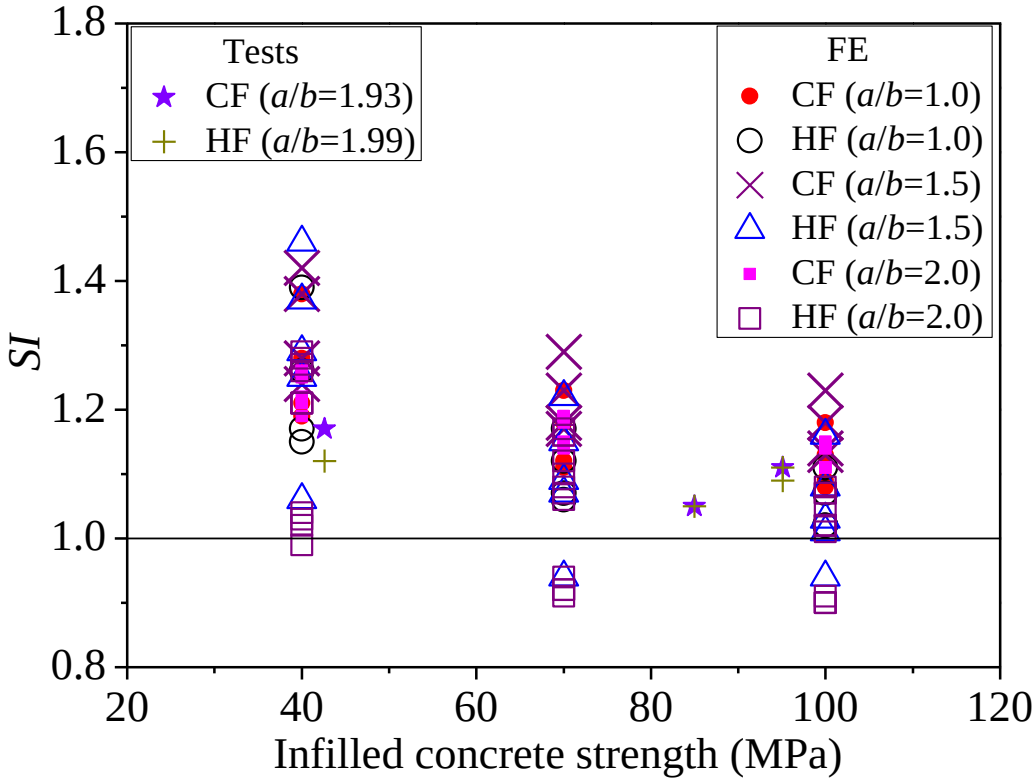

Figure 16: Effects of infilled concrete strength on strength enhancement index (***SI***) for different section aspect ratios

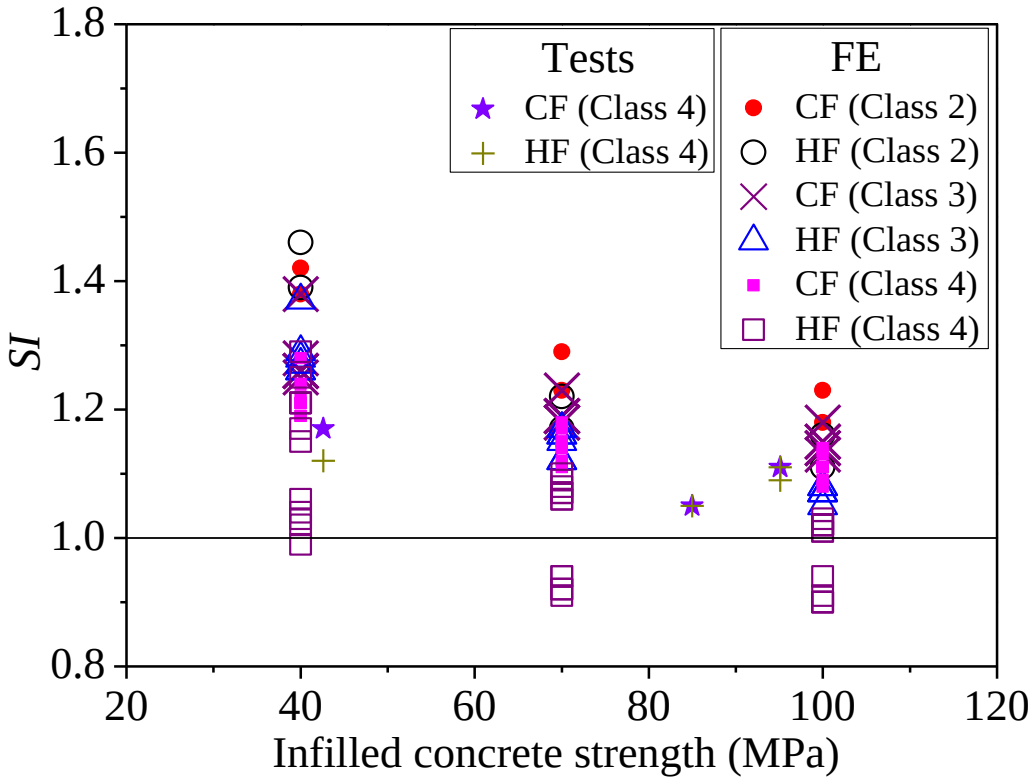

Figure 17: Effects of the infilled concrete strength on ***SI*** for different cross-section classes

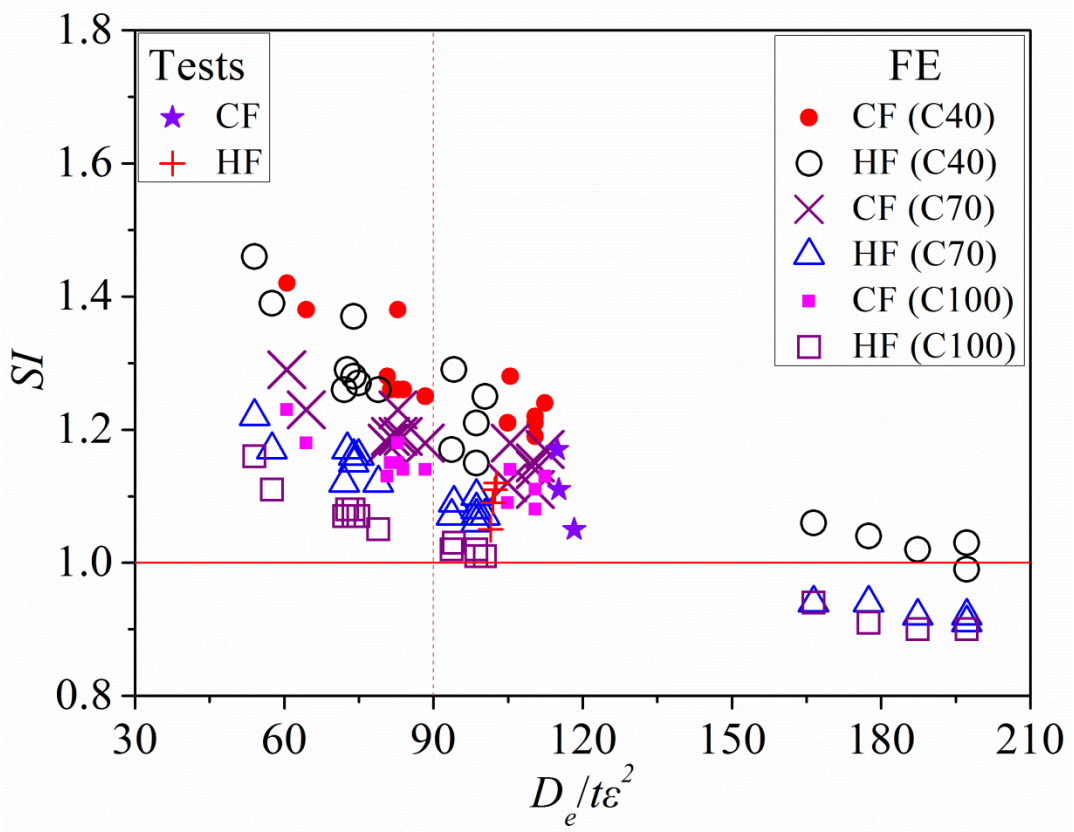

Figure 18: Effects of the section slenderness on ***SI*** for different infilled concrete strengths

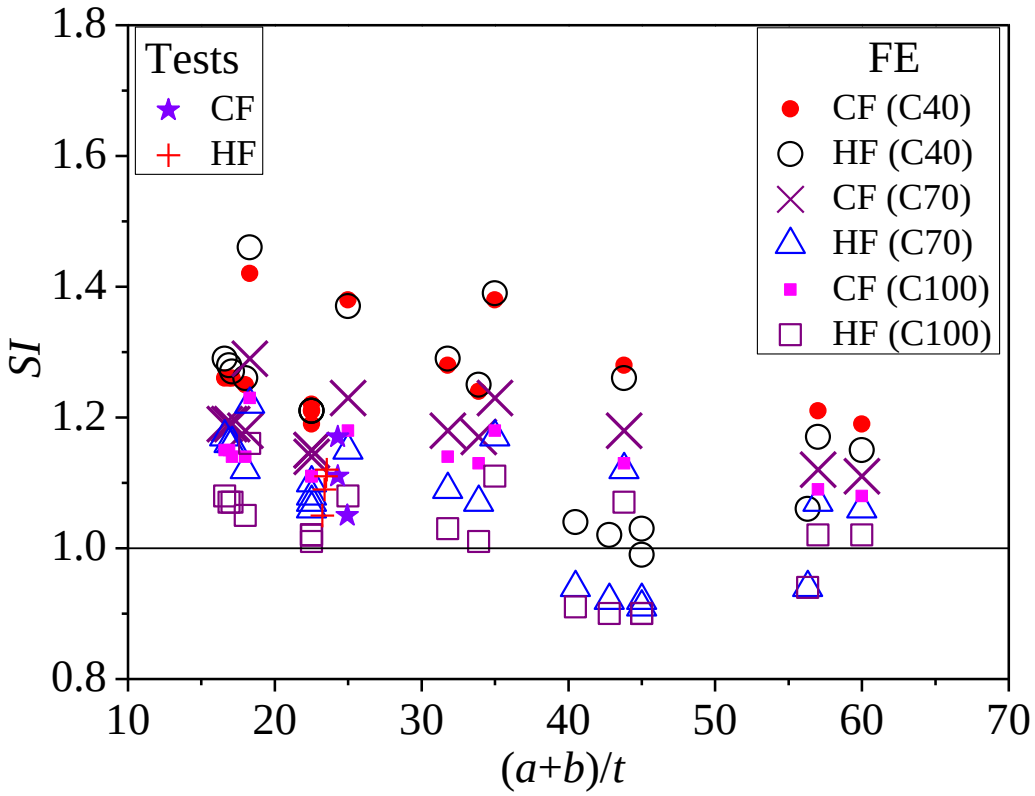

Figure 19: Effects of the section strength factor on ***SI*** for different infilled concrete strengths

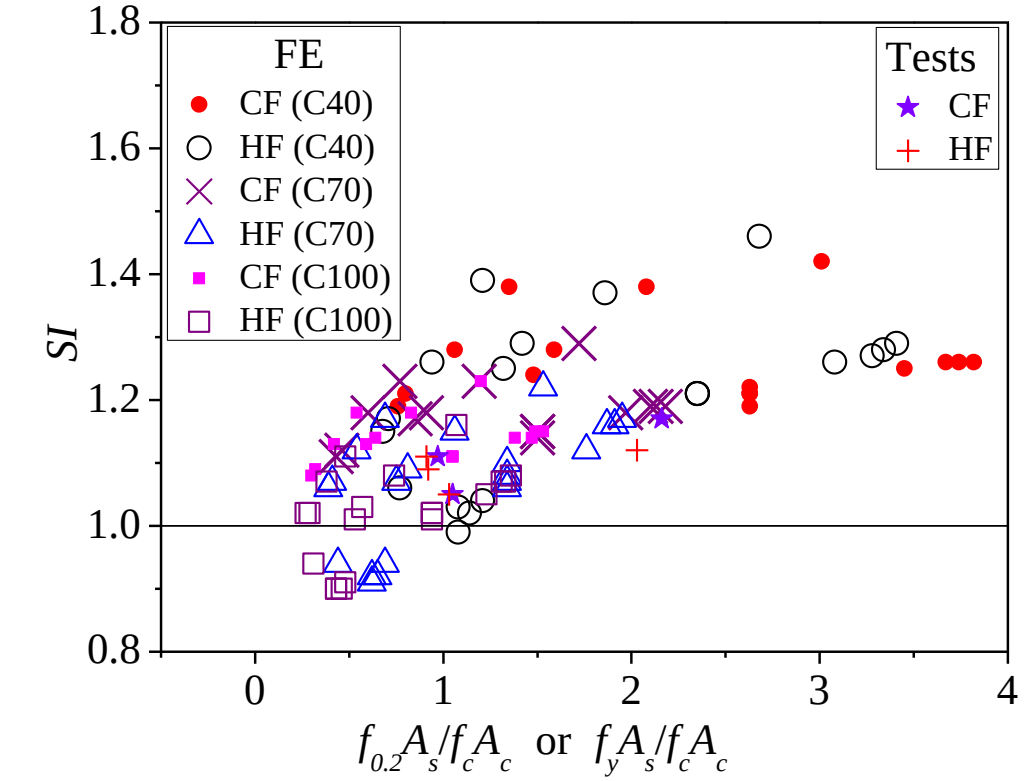

Figure 20: Effects of the section constraining factor on ***SI*** for different infilled concrete strengths

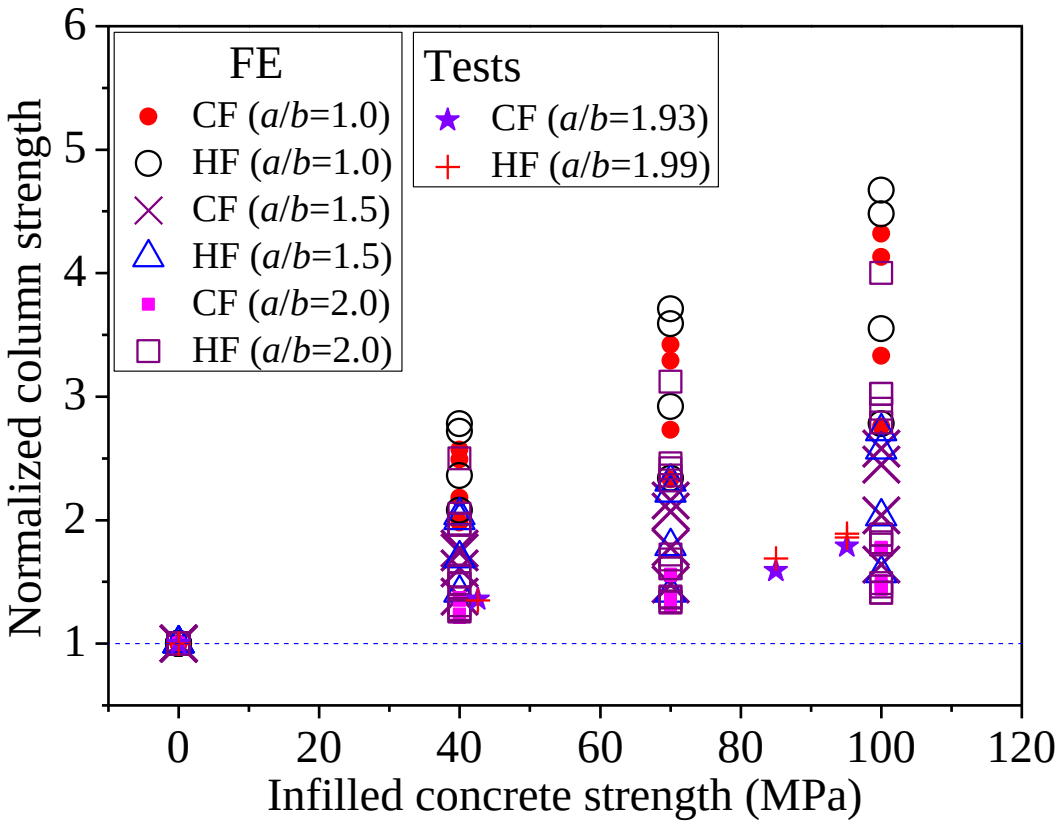

Figure 21: Comparison of column strength enhancement with different infilled concrete strengths and different section aspect ratios

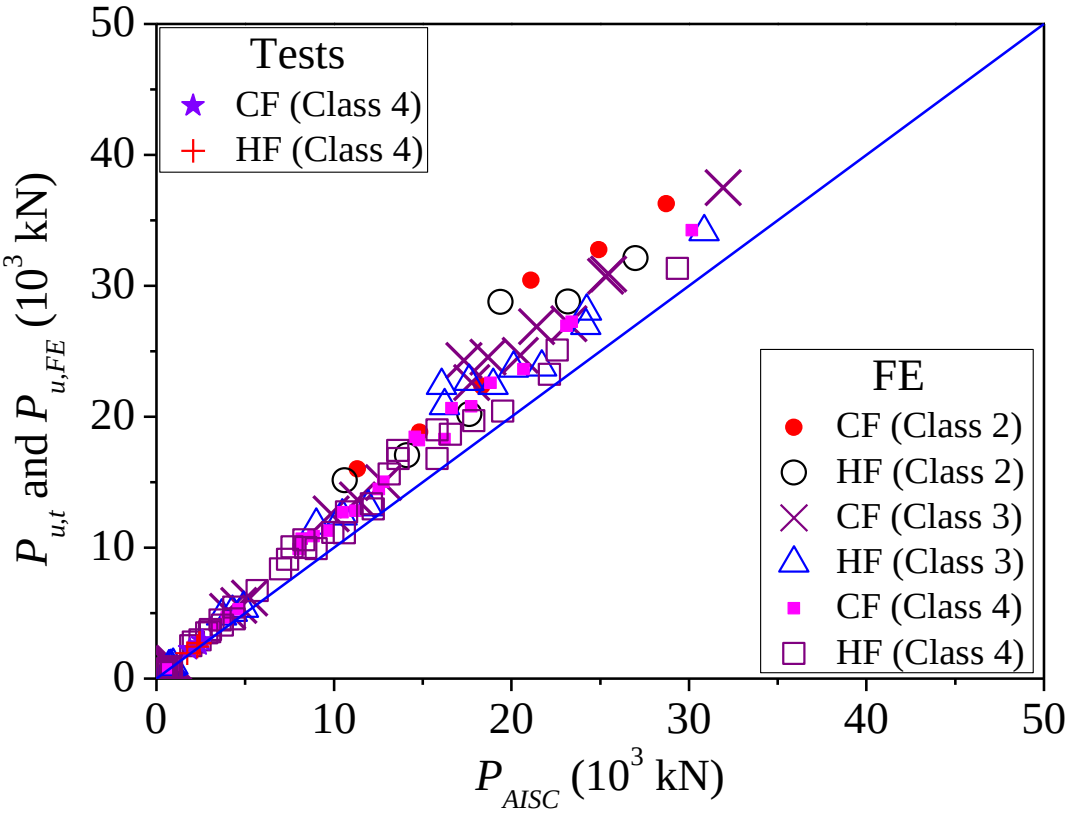

(a) For different cross-section classes of steel tubes (axes scale up to 50)

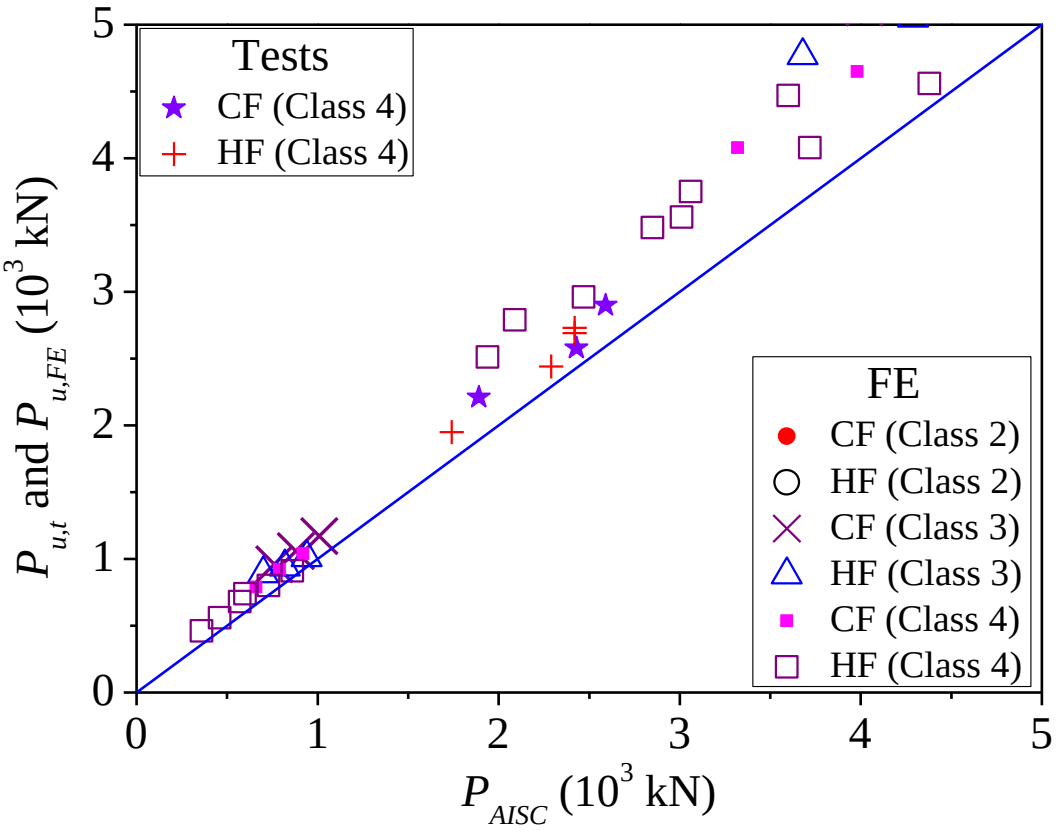

(b) For different cross-section classes of steel tubes (axes scale up to 5)

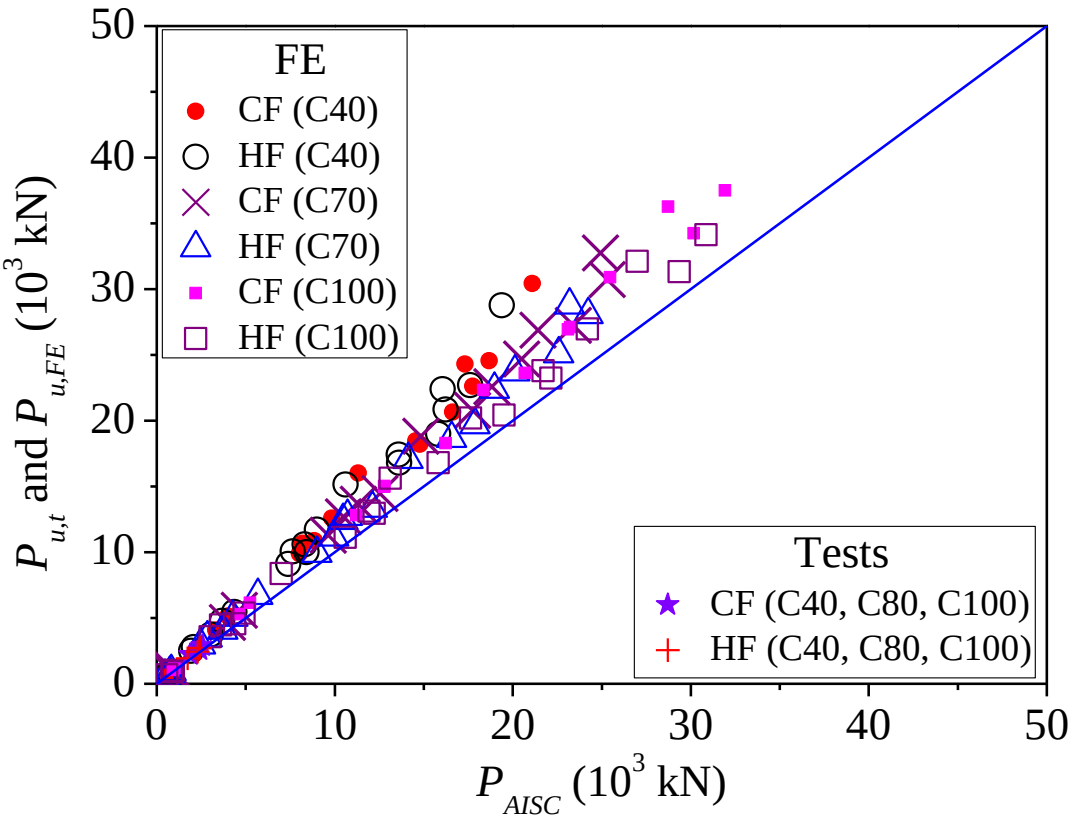

(c) For different infilled concrete grades

Figure 22: Comparison of test and FE results with nominal strengths predicted by AISC [4]

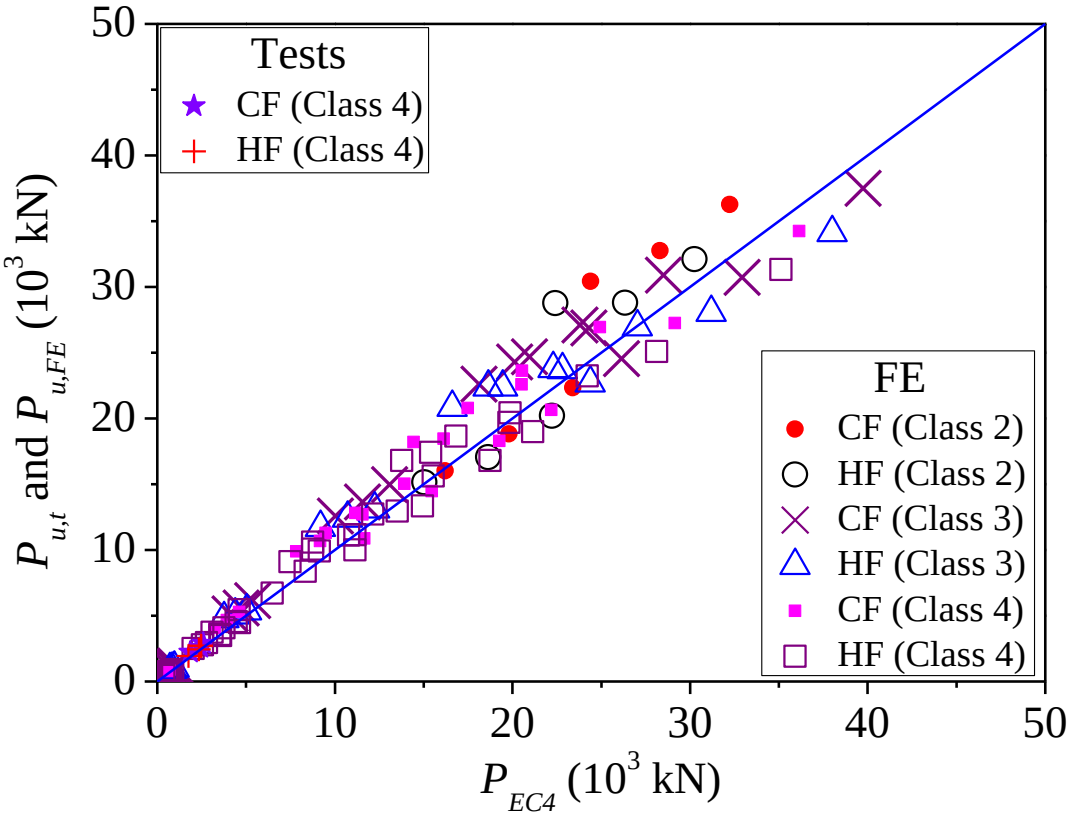

(a) For different cross-section classes of steel tubes (axes scale up to 50)

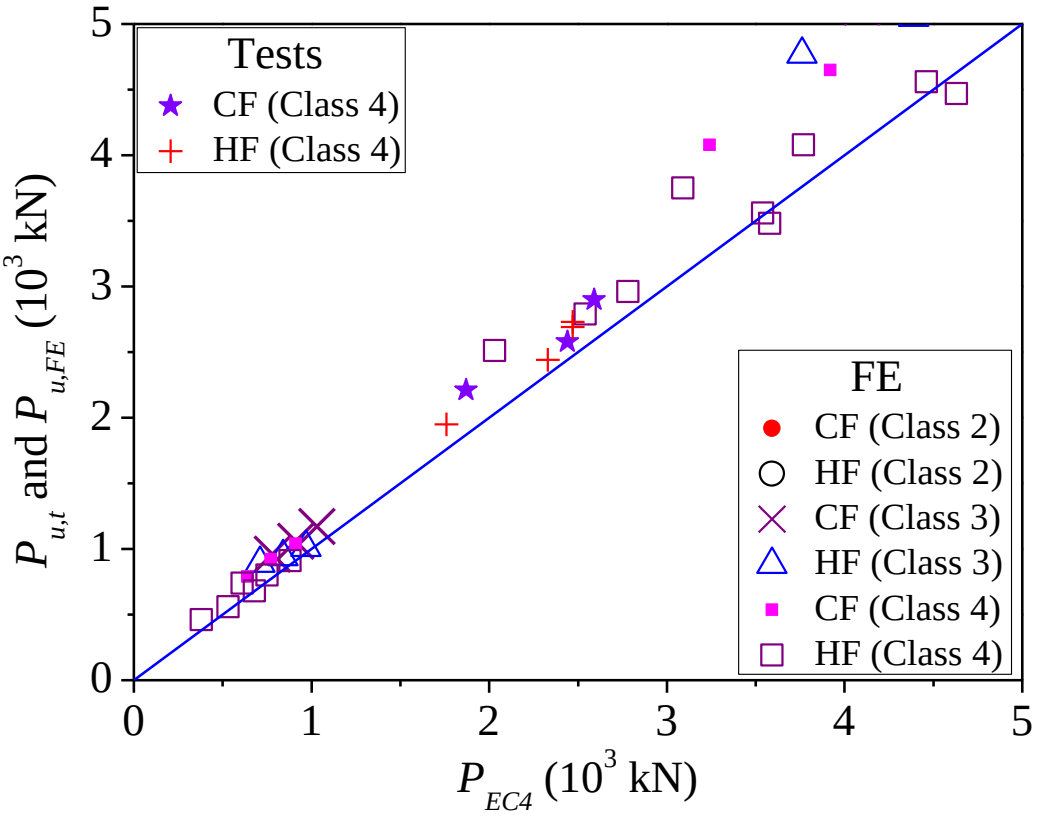

(b) For different cross-section classes of steel tubes (axes scale up to 5)

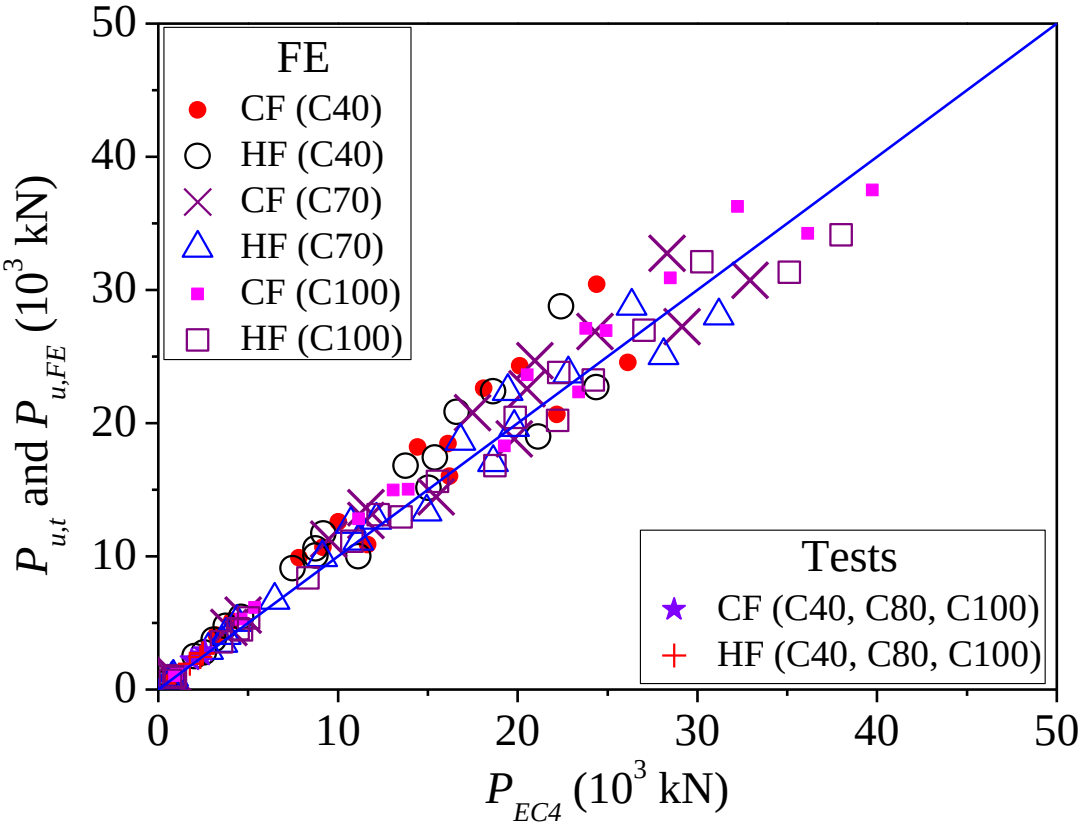

(c) For different infilled concrete grades

Figure 23: Comparison of test and FE results with nominal strengths predicted by EC4 [32]

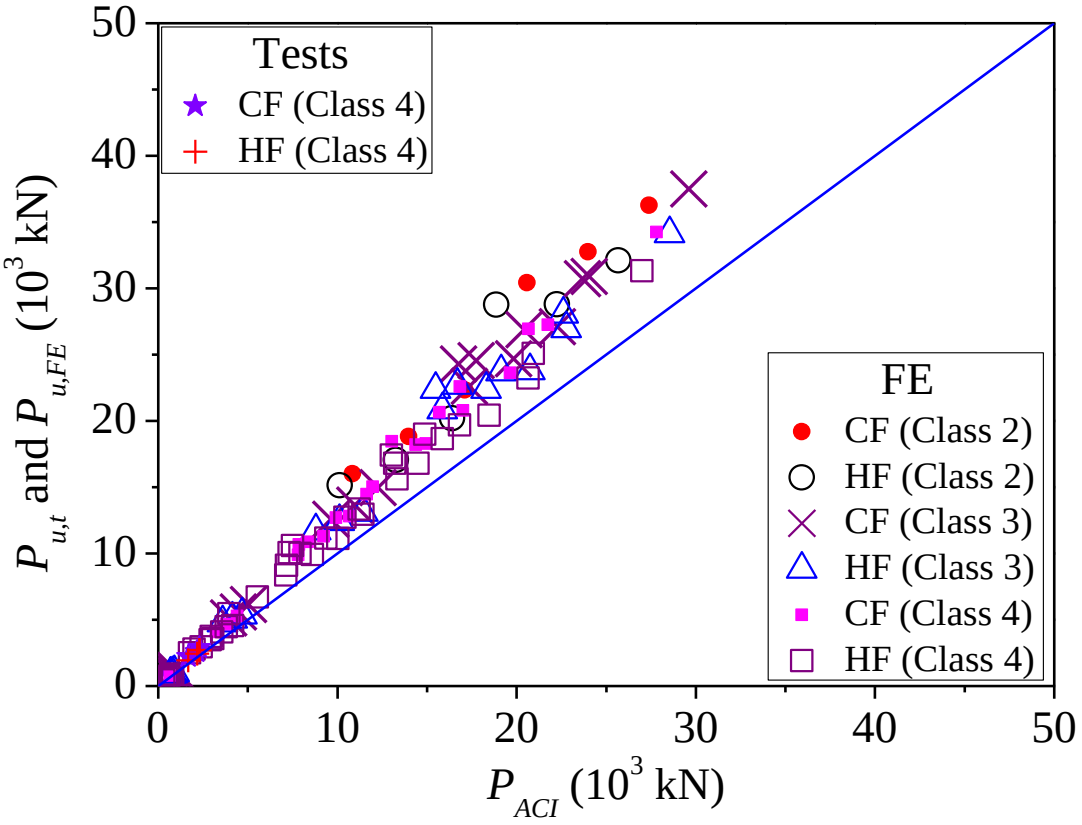

(a) For different cross-section classes of steel tubes (axes scale up to 50)

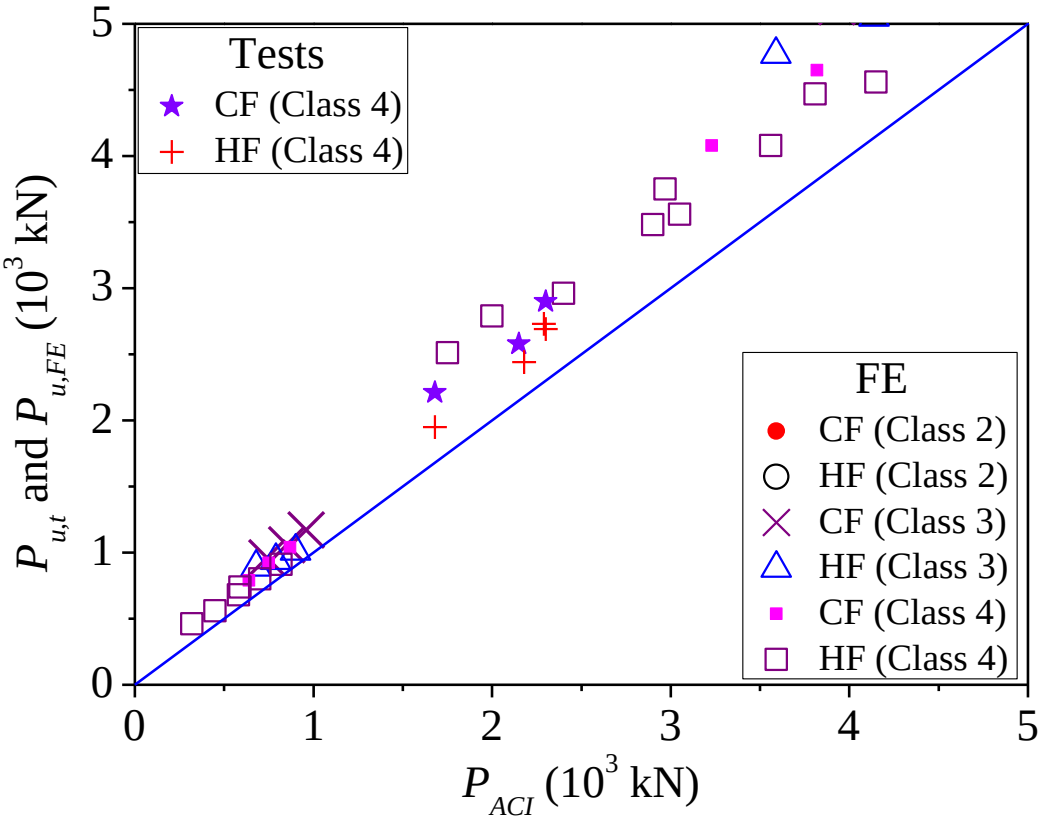

(b) For different cross-section classes of steel tubes (axes scale up to 5)

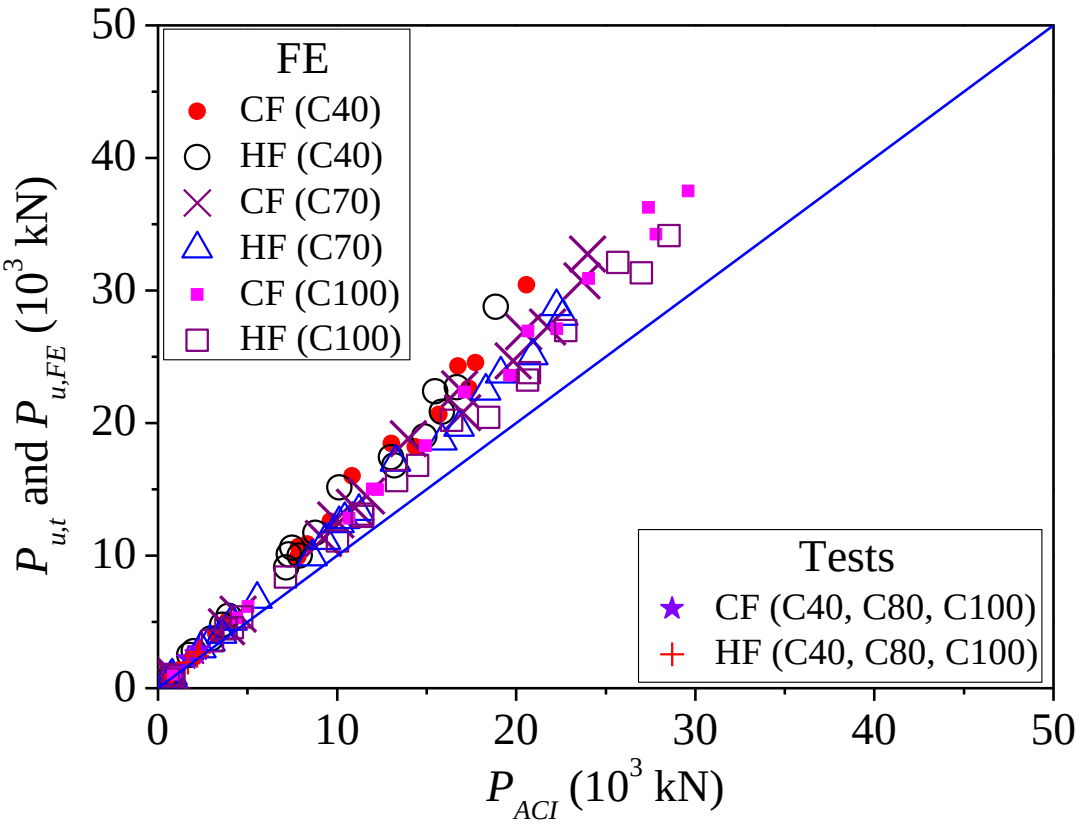

(c) For different infilled concrete grades

Figure 24: Comparison of test and FE results with nominal strengths predicted by ACI [33]

Table 1: Measured material properties of HF and CF EHS [24]

Steel type	Location	E_s (GPa)	$f_{0.2}$ (MPa)	f_y (MPa)	f_u (MPa)	ε_u (%)	ε_f (%)
CF	Flattest	201.1	432.6	-	571.9	11.6	29.9
	Curviest	196.6	465.4	-	589.0	7.3	25.8
	Mean	201.1	462.3	-	575.9	9.3	27.1
HF	Flattest	206.8	387.1	386.2	533.6	13.8	30.9
	Curviest	209.0	374.4	373.2	530.5	13.2	31.0
	Mean	206.3	382.3	383.2	537.6	12.4	30.8

Table 2: Test strengths of concrete cylinders

Concrete grade	Nominal strength (MPa)	Measured strength* (MPa)	
	f_{ck}	$f_{ck,28}$	$f_{ck,t}$
C40	40	37.2	42.6
C80	80	74.7	85.0
C100	100	89.7	95.1

Note: "*" reported in Ref. [34].

Table 3: Measured dimensions of stub column specimens

Steel type	Specimens	Measured value* (mm)				
		2a	*2b*	*t*	*L*	w_0
CF	200×100×6.5-40	204.3	105.7	6.38	330.0	-
	200×100×6.5-80	204.7	105.7	6.22	329.7	1.369
	200×100×6.5-100	204.4	105.5	6.38	330.0	-
HF	200×100×6.5-40	204.3	102.5	6.52	330.1	-
	200×100×6.5-80	204.4	102.5	6.60	330.3	0.116
	200×100×6.5-100	204.5	102.7	6.54	330.2	-
	200×100×6.5-100#	204.6	102.7	6.57	330.2	-

Note: "*" reported in Ref. [34].

Table 4: Test results and comparisons with FE predictions

Steel type	Specimens	$P_{u,t}$ (kN)	δ_u (mm)	$\delta_{u,0.85}$ (mm)	*Nor.*	$P_{u,FE}$ (kN)	$P_{u,t}/P_{u,FE}$
CF	200×100×6.5-0	1622.1*	-	-	1.00	-	-
	200×100×6.5-40	2205.6	3.4	13.2	1.36	2335.2	0.95
	200×100×6.5-80	2581.5	-	-	1.59	2796.1	0.92
	200×100×6.5-100	2902.5	1.7	2.0	1.79	2968.9	0.98
HF	200×100×6.5-0	1442.3*	-	-	1.00	-	-
	200×100×6.5-40	1947.7	2.0	>21	1.35	2093.7	0.93
	200×100×6.5-80	2441.3	1.5	1.7	1.69	2430.4	1.00
	200×100×6.5-100	2732.5	1.5	1.9	1.89	2534.3	1.08
	200×100×6.5-100#	2686.9	1.4	1.7	1.86	2530.2	1.06
						Mean	0.99
						COV	0.063

Note: "*" reported in Ref. [27]; "*Nor*." represents the $P_{u,t}$ normalized by that without infilled concrete in the same series.

Table 5: Values of parameters considered for concrete-filled HF and CF EHS stub columns

Section slenderness	$2a$ (mm)	t (mm)	a/b	Infilled concrete grades	D_e/t		Number	
					CF	HF	CF	HF
Class 2, Class 3, Class 4	120, 270, 420, 570	2.0 ~ 26.0	1.0, 1.5, 2.0	C40, C70, C100	32.9 ~ 57.0	32.9 ~ 120.0	48	63
						Total	111	

Table 6: Parameters and numerical results of concrete-filled steel stub columns with Class 2 cross-section ($50 < D_e/t\varepsilon^2 \leq 70$)

Specimens	a/b	Section area		CF			HF		
$2a\times2b\times t$		A_s	A_c	δ_u	$P_{u,FE}$	$\delta_{u,0.85}$	δ_u	$P_{u,FE}$	$\delta_{u,0.85}$
(mm)		10^3 (mm^2)	10^3 (mm^2)	(mm)	kN	(mm)	(mm)	kN	(mm)
420×420×12-0	1.0	15.38	123.16	18.5	8086*	37.2	26.2	7272*	46.4
420×420×12-40				86.8	16012	>200	89.6	15138	>200
420×420×12-70				10.7	18810	126.2	11.7	17044	>200
420×420×12-100				6.6	22334	20.3	8.8	20198	21.6
570×380×26-0	1.5	37.09	133.44	46.9	22061*	>50	60.2	20463*	>70
570×380×26-40				78.3	30423	>200	90.2	28769	>200
570×380×26-70				16.6	32759	>200	78.4	28804	>200
570×380×26-100				13.1	36267	96.3	13.2	32097	129.9

Note: "*" reported in Ref. [27].

Table 7: Parameters and numerical results of concrete-filled steel stub columns with Class 3 cross-section ($70 < D_e/t\varepsilon^2 \leq 90$)

Specimens	a/b	Section area		CF			HF		
$2a\times2b\times t$		A_s	A_c	δ_u	$P_{u,FE}$	$\delta_{u,0.85}$	δ_u	$P_{u,FE}$	$\delta_{u,0.85}$
(mm)		10^3 (mm^2)	10^3 (mm^2)	(mm)	kN	(mm)	(mm)	kN	(mm)
120×60×5-0	2.0	1.38	4.32	7.4	772*	10.9	7.2	677*	10.7
120×60×5-40				4.9	961	29.0	12.8	885	43.7
120×60×5-70				3.4	1057	25.2	13.6	937	39.1
120×60×5-100				2.9	1169	11.87	2.7	1011	19.6
270×135×12-0	2.0	7.41	21.45	19.7	4255*	26.6	18.7	3799*	26.8
270×135×12-40				11.5	5128	73.6	30.2	4769	>150
270×135×12-70				8.1	5580	45.92	34.9	5053	90.1
270×135×12-100				6.6	6141	39.6	6.2	5369	69.5
420×210×19-0	2.0	18.23	51.60	28.2	10421*	49.5	28.8	9286*	41.5
420×210×19-40				18.0	12576	112.6	45.0	11702	>200
420×210×19-70				12.6	13654	102.3	54.4	12414	136.6
420×210×19-100				10.3	14973	59.9	10.0	13118	106.2
570×570×13-0	1.0	22.75	232.43	20.3	11251*	33.8	22.3	9621*	37.6
570×570×13-40				26.1	24546	>200	94.1	22703	>200
570×570×13-70				10.1	30738	41.1	14.1	28049	>200
570×570×13-100				8.8	37494	25.3	13.6	34118	27.3
570×380×19-0	1.5	27.51	142.90	33.4	15117*	>50	34.9	13279*	>50
570×380×19-40				91.8	24305	127.3	94.1	22383	>200
570×380×19-70				13.1	26885	87.5	13.0	23704	>200
570×380×19-100				11.1	30893	16.3	12.3	26976	16.9
570×285×25-0	2.0	32.61	95.98	36.4	18488*	>50	36.4	16313*	>50
570×285×25-40				24.0	22600	137.1	62.0	20843	>200
570×285×25-70				17.1	24698	127.8	76.0	22404	182.3
570×285×25-100				13.6	27103	75.0	13.1	23783	136.5

Note: "*" reported in Ref. [27].

Table 8: Parameters and numerical results of concrete-filled steel stub columns with Class 4 cross-section ($D_e/t\varepsilon^2 > 90$)

Specimens	a/b	Section area		CF			HF		
$2a\times2b\times t$		A_s	A_c	δ_u	$P_{u,FE}$	$\delta_{u,0.85}$	δ_u	$P_{u,FE}$	$\delta_{u,0.85}$
(mm)		10^3 (mm^2)	10^3 (mm^2)	(mm)	kN	(mm)	(mm)	kN	(mm)
120×60×4-0	2.0	1.11	4.57	6.2	587*	10.2	5.6	497*	11.8
120×60×4-40				7.2	793	32.5	12.1	741	>80
120×60×4-70				2.9	918	21.0	3.0	799	37.5
120×60×4-100				2.4	1044	4.1	2.6	905	4.5
270×135×9-0	2.0	5.64	23.16	13.5	2989*	22.9	12.7	2538*	26.0
270×135×9-40				9.2	4078	35.5	25.7	3745	83.7
270×135×9-70				6.6	4647	31.3	30.4	4075	83.0
270×135×9-100				5.6	5285	9.2	5.8	4557	12.1
420×420×7-0	1.0	9.08	129.46	8.2	4234*	13.6	2.1	3597*	12.5
420×420×7-40				16.2	10862	>150	22.2	10001	>150
420×420×7-70				6.6	14482	26.2	10.2	13344	29.1
420×420×7-100				5.6	18284	17.3	8.8	16807	18.7
420×280×11-0	1.5	11.84	80.65	18.2	6132*	43.7	13.2	5031*	24.6
420×280×11-40				58.6	10675	87.2	73.2	10073	93.2
420×280×11-70				8.0	12695	57.9	9.1	11153	>150
420×280×11-100				6.9	15031	10.6	8.0	12954	11.3
420×210×14-0	2.0	13.64	56.03	20.2	7236*	>50	13.8	5902*	20.5
420×210×14-40				14.6	9896	68.6	42.9	9100	108.9
420×210×14-70				10.2	11297	77.0	52.6	9919	95.9
420×210×14-100				8.6	12820	13.3	9.2	11108	59.7
570×570×10-0	1.0	17.59	237.58	12.8	8287*	21.5	5.4	6992*	22.6
570×570×10-40				22.1	20642	>200	30.1	18989	>200
570×570×10-70				8.8	27256	36.2	13.6	25076	40.5
570×570×10-100				7.5	34233	23.7	10.7	31314	25.6
570×380×14-0	1.5	20.49	149.84	22.9	10441*	>50	15.4	8522	28.6
570×380×14-40				73.7	18454	111.1	86.8	17422*	117.8
570×380×14-70				10.3	22582	29.2	12.2	19694	>200
570×380×14-100				9.3	26943	14.1	9.2	23217	15.4
570×285×19-0	2.0	25.13	103.20	27.4	13308*	>50	18.4	10851*	27.4
570×285×19-40				19.1	18211	112.0	54.6	16803	>200
570×285×19-70				14.0	20791	115.8	78.5	18641	177.8
570×285×19-100				11.4	23607	18.5	12.3	20422	18.2

Note: "*" reported in Ref. [27].

Table 9: Parameters and numerical results of concrete-filled HF steel stub columns with Class 4 cross-section ($D_e/t\varepsilon^2 > 90$)

Specimens	a/b	Section area		HF		
$2a\times2b\times t$		A_s	A_c	δ_u	$P_{u,FE}$	$\delta_{u,0.85}$
(mm)		10^3 (mm^2)	10^3 (mm^2)	(mm)	kN	(mm)
120×60×2-0	2.0	0.57	5.10	0.6	226*	3.0
120×60×2-40				13.1	463	>60
120×60×2-70				2.7	555	>60
120×60×2-100				1.8	683	3.2
270×180×4-0	1.5	2.81	35.39	1.6	1116*	5.1
270×180×4-40				44.6	2787	>100
270×180×4-70				4.9	3479	>100
270×180×4-100				3.4	4465	6.1
270×135×5-0	2.0	3.19	25.53	1.7	1277*	6.8
270×135×5-40				27.8	2505	>100
270×135×5-70				5.9	2964	>100
270×135×5-100				4.1	3561	7.6
420×210×7-0	2.0	6.97	62.50	1.9	2772*	7.0
420×210×7-40				31.9	5454	>150
420×210×7-70				7.8	6713	48.1
420×210×7-100				6.2	8364	11.1
570×285×10-0	2.0	13.50	114.47	2.7	5391*	14.5
570×285×10-40				56.0	10591	>200
570×285×10-70				10.7	12718	93.0
570×285×10-100				8.3	15633	15.0

Note: "*" reported in Ref. [27].

Table 10: Comparisons of the behavior for concrete-filled steel stub columns with Class 2 cross-section ($50 < D_e/t\varepsilon^2 \leq 70$)

Specimens	α	γ	CF				HF			
$2a\times2b\times t$ (mm)	a/b	$(a+b)/t$	ξ	***SI***	***DI***	*Nor.*	ξ	***SI***	***DI***	*Nor.*
420×420×12-0	1.0	35.0	-	-	2.01	1.00	-	-	1.77	1.00
420×420×12-40			1.35	1.38	>2.30	1.98	1.21	1.39	>2.23	2.08
420×420×12-70			0.77	1.23	11.79	2.33	0.69	1.17	>17.09	2.34
420×420×12-100			0.54	1.18	3.08	2.76	0.48	1.11	2.45	2.78
570×380×26-0	1.5	18.3	-	-	>1.07	1.00	-	-	>1.16	1.00
570×380×26-40			3.01	1.42	>2.55	1.38	2.68	1.46	>2.22	1.41
570×380×26-70			1.72	1.29	>12.05	1.48	1.53	1.22	>2.55	1.41
570×380×26-100			1.20	1.23	7.35	1.64	1.07	1.16	9.84	1.57

Note: "*Nor.*" represents the $P_{u,FE}$ normalized by that without infilled concrete in the same series.

Table 11: Comparisons of the behavior for concrete-filled steel stub columns with Class 3 cross-section ($70 < D_e/t\varepsilon^2 \leq 90$)

Specimens	α	γ	CF				HF			
$2a\times2b\times t$ (mm)	a/b	$(a+b)/t$	ξ	***SI***	***DI***	*Nor.*	ξ	***SI***	***DI***	*Nor.*
120×60×5-0	2.0	18.0	-	-	1.47	1.00	-	-	1.49	1.00
120×60×5-40			3.45	1.25	5.92	1.24	3.08	1.26	3.41	1.31
120×60×5-70			1.97	1.18	7.41	1.37	1.76	1.12	2.88	1.38
120×60×5-100			1.38	1.14	4.09	1.51	1.23	1.05	7.26	1.49
270×135×12-0	2.0	16.9	-	-	1.35	1.00	-	-	1.43	1.00
270×135×12-40			3.74	1.26	6.40	1.21	3.34	1.28	>4.97	1.26
270×135×12-70			2.13	1.19	5.67	1.31	1.91	1.16	2.58	1.33
270×135×12-100			1.49	1.15	6.00	1.44	1.33	1.07	11.21	1.41
420×210×19-0	2.0	16.6	-	-	1.76	1.00	-	-	1.44	1.00
420×210×19-40			3.82	1.26	6.26	1.21	3.41	1.29	>4.44	1.26
420×210×19-70			2.18	1.19	8.12	1.31	1.95	1.17	2.51	1.34
420×210×19-100			1.53	1.15	5.82	1.44	1.36	1.08	10.62	1.41
570×570×13-0	1.0	43.8	-	-	1.67	1.00	-	-	1.69	1.00
570×570×13-40			1.06	1.28	>7.66	2.18	0.94	1.26	>2.13	2.36
570×570×13-70			0.60	1.18	4.07	2.73	0.54	1.12	>14.18	2.92
570×570×13-100			0.42	1.13	2.88	3.33	0.38	1.07	2.01	3.55
570×380×19-0	1.5	25.0	-	-	>1.50	1.00	-	-	>1.43	1.00
570×380×19-40			2.08	1.38	1.39	1.61	1.86	1.37	>2.13	1.69
570×380×19-70			1.19	1.23	6.68	1.78	1.06	1.15	>15.38	1.79
570×380×19-100			0.83	1.18	1.47	2.04	0.74	1.08	1.37	2.03
570×285×25-0	2.0	17.1	-	-	>1.37	1.00	-	-	>1.37	1.00
570×285×25-40			3.67	1.26	5.71	1.22	3.28	1.27	>3.23	1.28
570×285×25-70			2.10	1.19	7.47	1.34	1.87	1.16	2.40	1.37
570×285×25-100			1.47	1.14	5.51	1.47	1.31	1.07	10.42	1.46

Note: "*Nor.*" represents the $P_{u,FE}$ normalized by that without infilled concrete in the same series.

Table 12: Comparisons of the behavior for concrete-filled steel stub columns with Class 4 cross-section ($D_e/t\varepsilon^2 > 90$)

Specimens	α	γ	CF				HF			
$2a\times2b\times t$ (mm)	a/b	$(a+b)/t$	ξ	***SI***	***DI***	*Nor.*	ξ	***SI***	***DI***	*Nor.*
120×60×4-0	2.0	22.5	-	-	1.65	1.00	-	-	2.11	1.00
120×60×4-40			2.63	1.19	4.51	1.35	2.35	1.21	6.61	1.49
120×60×4-70			1.50	1.14	7.24	1.56	1.34	1.06	12.50	1.61
120×60×4-100			1.05	1.11	1.71	1.78	0.94	1.02	1.73	1.82
270×135×9-0	2.0	22.5	-	-	1.70	1.00	-	-	2.05	1.00
270×135×9-40			2.63	1.21	3.86	1.36	2.35	1.21	3.26	1.48
270×135×9-70			1.50	1.14	4.74	1.55	1.34	1.07	2.73	1.61
270×135×9-100			1.05	1.11	1.64	1.77	0.94	1.01	2.09	1.80
420×420×7-0	1.0	60.0	-	-	1.66	1.00	-	-	5.95	1.00
420×420×7-40			0.76	1.19	>9.26	2.57	0.68	1.15	>6.76	2.78
420×420×7-70			0.43	1.11	3.97	3.42	0.39	1.06	2.85	3.71
420×420×7-100			0.30	1.08	3.09	4.32	0.27	1.02	2.13	4.67
420×280×11-0	1.5	31.8	-	-	2.40	1.00	-	-	1.86	1.00
420×280×11-40			1.59	1.28	1.49	1.74	1.42	1.29	1.27	2.00
420×280×11-70			0.91	1.18	7.24	2.07	0.81	1.09	>16.48	2.22
420×280×11-100			0.64	1.14	1.54	2.45	0.57	1.03	1.41	2.57
420×210×14-0	2.0	22.5	-	-	>2.48	1.00	-	-	1.49	1.00
420×210×14-40			2.63	1.22	4.70	1.37	2.35	1.21	2.54	1.54
420×210×14-70			1.50	1.15	7.55	1.56	1.34	1.08	1.82	1.68
420×210×14-100			1.05	1.11	1.55	1.77	0.94	1.02	6.49	1.88
570×570×10-0	1.0	57.0	-	-	1.68	1.00	-	-	4.19	1.00
570×570×10-40			0.80	1.21	>9.05	2.49	0.71	1.17	>6.64	2.72
570×570×10-70			0.46	1.12	4.11	3.29	0.41	1.07	2.98	3.59
570×570×10-100			0.32	1.09	3.16	4.13	0.29	1.02	2.39	4.48
570×380×14-0	1.5	33.9	-	-	>2.18	1.00	-	-	1.86	1.00
570×380×14-40			1.48	1.24	1.51	1.77	1.32	1.25	1.36	2.04
570×380×14-70			0.85	1.17	2.83	2.16	0.75	1.07	>16.39	2.31
570×380×14-100			0.59	1.13	1.52	2.58	0.53	1.01	1.67	2.72
570×285×19-0	2.0	22.5	-	-	>1.82	1.00	-	-	1.49	1.00
570×285×19-40			2.63	1.21	5.86	1.37	2.35	1.21	>3.66	1.55
570×285×19-70			1.50	1.15	8.27	1.56	1.34	1.10	2.26	1.72
570×285×19-100			1.05	1.11	1.62	1.77	0.94	1.02	1.48	1.88

Note: "*Nor.*" represents the $P_{u,FE}$ normalized by that without infilled concrete in the same series.

Table 13: Comparisons of the behavior for concrete-filled steel stub columns with Class 4 cross-section ($D_e/t\varepsilon^2 > 90$)

Specimens	α	γ	HF			
$2a\times2b\times t$ (mm)	a/b	$(a+b)/t$	ξ	***SI***	***DI***	*Nor.*
120×60×2-0	2.0	45.0	-	-	5.00	1.00
120×60×2-40			1.08	1.03	>4.58	2.05
120×60×2-70			0.62	0.92	>22.22	2.46
120×60×2-100			0.43	0.90	1.78	3.02
270×180×4-0	1.5	56.3	-	-	3.19	1.00
270×180×4-40			0.77	1.06	>2.24	2.50
270×180×4-70			0.44	0.94	>20.41	3.12
270×180×4-100			0.31	0.94	1.79	4.00
270×135×5-0	2.0	40.5	-	-	4.00	1.00
270×135×5-40			1.21	1.04	>3.60	1.96
270×135×5-70			0.69	0.94	>16.95	2.32
270×135×5-100			0.48	0.91	1.85	2.79
420×210×7-0	2.0	45.0	-	-	3.68	1.00
420×210×7-40			1.08	0.99	>4.70	1.97
420×210×7-70			0.62	0.91	6.17	2.42
420×210×7-100			0.43	0.90	1.79	3.02
570×285×10-0	2.0	42.8	-	-	5.37	1.00
570×285×10-40			1.14	1.02	>3.57	1.96
570×285×10-70			0.65	0.92	8.69	2.36
570×285×10-100			0.46	0.90	1.81	2.90

Note: "*Nor.*" represents the $P_{u,FE}$ normalized by that without infilled concrete in the same series.

Table 14: Comparisons of test and numerical ultimate strengths with nominal strengths predicted by different design specifications

(a) For different cross-section classes of steel tubes

Cases		CF specimens				HF specimens			
		No. of columns	P_u/P_{AISC}	P_u/P_{EC4}	P_u/P_{ACI}	No. of columns	P_u/P_{AISC}	P_u/P_{EC4}	P_u/P_{ACI}
Infilled concrete with Class 2 steel tube	Mean	6	1.32	1.07	1.38	6	1.28	1.04	1.35
	COV		0.068	0.115	0.055		0.108	0.133	0.096
Infilled concrete with Class 3 steel tube	Mean	18	1.23	1.14	1.28	18	1.19	1.10	1.24
	COV		0.051	0.091	0.048		0.078	0.110	0.070
Infilled concrete with Class 4 steel tube	Mean	27	1.18	1.11	1.26	43	1.16	1.05	1.22
	COV		0.044	0.098	0.043		0.073	0.097	0.077
All cases	Mean	51	1.21	1.12	1.28	67	1.18	1.07	1.24
	COV		0.061	0.097	0.054		0.082	0.105	0.082

(b) For different infilled concrete grades

Cases		CF specimens				HF specimens			
		No. of columns	P_u/P_{AISC}	P_u/P_{EC4}	P_u/P_{ACI}	No. of columns	P_u/P_{AISC}	P_u/P_{EC4}	P_u/P_{ACI}
Infilled concrete C40	Mean	17	1.28	1.16	1.34	22	1.28	1.16	1.35
	COV		0.059	0.110	0.057		0.062	0.104	0.066
Infilled concrete C70	Mean	17	1.20	1.10	1.27	22	1.15	1.04	1.20
	COV		0.045	0.092	0.040		0.043	0.080	0.036
Infilled concrete C100	Mean	17	1.17	1.08	1.24	23	1.11	1.00	1.16
	COV		0.031	0.075	0.033		0.054	0.063	0.034
All cases	Mean	51	1.21	1.12	1.28	67	1.18	1.07	1.24
	COV		0.061	0.097	0.054		0.082	0.105	0.082